



Universita' degli Studi di Napoli Federico II
Scuola di Dottorato in Ingegneria Industriale
Dottorato di Ricerca in Ingegneria Chimica - XXVII ciclo

3D finite volume simulations of dense granular flow inside rotating cylinders

Tesi di Dottorato di

Gaetano De Monaco

Comitato Scientifico

prof. ing. **Pier Luca Maffettone**
Universita' degli Studi di Napoli Federico II

dr. **Francesco Greco**
Istituto di Ricerche sulla Combustione — CNR

prof. ing. **Piero Salatino**
Universita' degli Studi di Napoli Federico II

*Who, then, can calculate the course of a molecule?
How do we know that the creation of worlds is not
determined by the fall of grains of sand?*

Victor Hugo — Les misérables

Abstract

Granular materials are widely diffused in industry as well as in nature, but a reliable and effective description of their motion is still at a rather early stage of development. Among the benchmark problems of granular dense flow, the rotating drum is one of the most challenging, yet intriguing and technologically relevant. In proper ranges of operating conditions, granular materials inside rotating drums display a continuum motion near their free surface. The motion of those discrete systems has been studied both experimentally and through Discrete Element Method (DEM) numerical simulations; however, it can also be regarded as the flow of a continuum medium, thus allowing a continuum mechanics approach.

In this thesis, we solve the continuum dynamic equations by adopting the visco-plastic JFP constitutive model (Jop et al., Nature 441, 727–730, 2006) for the stress tensor, and study the continuous flow of dry grains inside axially rotating cylinders through 3D Finite Volume simulations (FVM). We investigate the effect of the ratio D/d_p between the diameters of cylinder and particles, of the aspect ratio of the cylinder $AR = width/diameter$, of the angular velocity Ω , and of the slip between drum wall and particles.

Numerical results are found to quantitatively agree with experimental results from different authors, and also catches some distinctive features of the drum flow of granular materials, such as, e.g., the existence of axial components of the surface velocity, or the differences of the flow fields near the lateral wall and at the center plane, ect.

Our simulations demonstrate that the basic physics of the dense granular flow is captured by the simple JFP model, and that continuum mechanics can be used to get a physical insight in granular dense state phenomenology. CFD simulations may then be of help to rationalize the broad wealth of experimental results with these materials.

Contents

List of figures	iii
1 Introduction	1
1.1 Work motivation	4
2 Literature overview	5
2.1 Generalities on rotating cylinders	5
2.2 Review of experimental literature	9
2.3 Review of numerical literature	19
2.3.1 Discrete approaches	20
2.4 Review of theoretical literature	23
2.5 JFP model	28
3 Materials and methods	41
3.1 Materials and geometries	41
3.2 Governing equations	43
3.3 Numerical method	49
3.4 Convergence tests	52
4 Results	56
4.1 Introduction	56
4.2 Free-surface	58

4.3	Flowing layer thickness	59
4.3.1	AR and slip effects	62
4.4	Dynamic angle	64
4.5	Velocity profiles	67
4.6	Inertial number profiles	70
4.7	Surface velocity	71
4.8	Discussion	74
5	Conclusions	81
	Bibliography	85

List of Figures

1.1	Steel beads on an inclined plane	2
2.1	Flow configurations table	6
2.2	Sketch of the geometry and of the flow	8
2.3	Sketch of the free-surface profile	10
2.4	Density plots of the axial velocity on the free-surface of the flowing layer for various AR	13
2.5	The streamwise surface velocity as a function of the axial position	15
2.6	Velocity profiles measured with MRI and PEPT	18
2.7	Variation of the starting and stopping angle with h	30
2.8	Diagram of the granular flow regimes	31
2.9	Friction coefficient and volume fraction as a function of the inertial number	33
2.10	Effective friction coefficient and packing fraction as a function of I	34
2.11	Two snapshots of a falling column 3D flow at two different times	37
3.1	Sketch of the polygonal mesh for $AR = 1$	53
3.2	Temporal evolutions to assess convergence	54
4.1	Cut of the granular phase and sampling lines	57
4.2	The free surfaces at the center of the cylinder	58

4.3	Thickness of the flowing layer versus Ω	60
4.4	Ratio between the thicknesses of the flowing layer near the wall and at the center versus AR	61
4.5	Axial profiles of the thickness of the flowing layer parametric in Ω	62
4.6	Effect of the aspect ratio AR on the flow depth	63
4.7	Axial profiles of the thickness of the flowing layer parametric in Ω	64
4.8	Dynamic angle versus Ω	65
4.9	Axial profile of the dynamic angle parametric in Ω	66
4.10	Axial profile of the dynamic angle parametric in AR	67
4.11	Radial velocity profiles at center and near the wall parametric in Ω	68
4.12	Radial velocity profiles at center and near the wall parametric in AR and β	69
4.13	Axial profiles of the velocity parametric in Ω	70
4.14	Radial profiles of the inertial number at center and near the wall parametric in Ω	71
4.15	Contours of the free-surface velocity parametric in Ω	72
4.16	Contours of the free-surface velocity parametric in β	73
4.17	Comparison between numerical results and experimental data on the flowing layer thickness.	75
4.18	Comparison between numerical results and experimental data on the free-surface velocity at the center plane	76
4.19	Comparison between numerical results and experimental axial velocity profiles	77
4.20	Time evolution of the axial velocity profile for the no-slip case	78
4.21	Velocity profiles with various cutoff viscosities	79

Granular materials are widely diffused in industry as well as in nature. It has been estimated that more than 50% of sales in the world involve commodities produced using granular materials at some stage, which makes granular media the second most used type of material in industry after water (Andreotti et al., 2013). The fields of interest for granular materials are numerous and their application ranges from pharmaceutical (Khalilitehrani et al., 2013) to food industries, from geophysics to planetary science, from ores to polymers processing (Meier et al., 2007).

Industries dealing with such materials often rely on trial and error experimental protocols and on the experience gained in their particular process. Indeed, granular materials still lack a unified theoretical framework and their proper description is still today an edge–problem in physics (Science2005). Those difficulties do not (only) depend on the great variety of such materials, since they arise even with “model granular media”, like hard spherical mono–disperse discrete systems in flow: granular macroscopic behaviors are not clearly linked to particles interactions (GDR MiDi, 2004; Ottino, 2006)

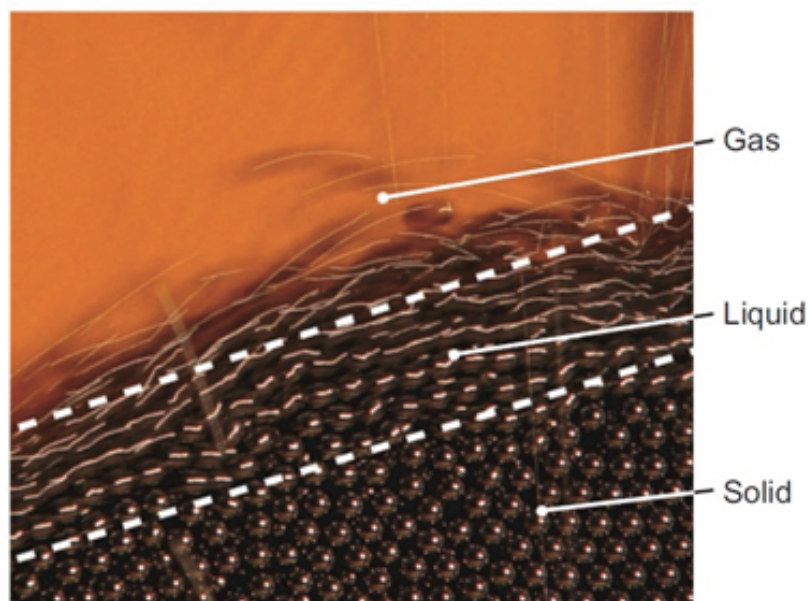


Figure 1.1: Steel beads on an inclined plane. Three regimes are simultaneously present: the bouncing spheres on top behave like gaseous “molecules”; the “flowing” beads in the middle resemble usual fluids and the jammed beads at the bottom behave like an elastic solid. From Forterre and Pouliquen (2008).

and a clear-cut length/time scales separation might be lacking in such systems (Andreotti et al., 2013), as it seems to be suggested by (e.g.) the observed formation of clusters with dimensions going from grain size up to the dimension of the flow (Bonamy et al., 2002a).

Besides their industrial importance, granular materials represent an exciting challenge in physics since the very first work of Coulomb, who investigated the stability of granular heap in 1773 (Andreotti et al., 2013). More than two centuries later, Osborne Reynolds said: *“I have in my hand the first experimental model universe, a soft India rubber bag filled with small shot”*. Indeed, part of their charm comes from their ability to mimic differ-

ent states of matter: they can act like gas, liquid, solids (see Figure 1.1) and they can even show glassy behaviors. When sheared, granular materials can expand, showing a rate-dependent dilatancy (Reynolds, 1885; Faqih et al., 2006) that might depend on the inter-grain friction (Peyneau and Roux, 2008). In addition, the behaviors of a granular system can depend upon its past history (Ottino, 2006; Kadanoff, 1999; Andreotti et al., 2013; Zheng and Yu, 2014). The dynamics of such materials, which Jaeger et al. (1996) addressed as “*unusual*”, is still as elusive as when de Gennes (1999) said “[...] *even for the simplest “dry” systems, the statistical physics of grains is still in its infancy. [...] The link between mechanics, tribology, statistical physics, surface chemistry, ... remains to be built*”.

Despite all the difficulties, some theoretical advances have been made, especially for the cases of granular solids, i.e. in the dense quasi-static regime in which the deformations are very slow and the particles interact by prolonged frictional contacts (Roux and Combe, 2002), and in granular gases, in which the flow is very rapid and dilute, and the particles interact by collisions (Goldhirsch, 2003). In contrast with the solid and gaseous behaviors, the theory for dense liquid regime, in which the material flows in a liquid-like way, is still at a rather early stage of development.

In the absence of a solid theoretical framework for granular dense flow, many descriptions rely on numerical simulation or on analytical simplified models. Even if granular materials seem tailor-made for a discrete viewpoint description, there is a great debate in literature on whether a continuum description, especially through fluid-like dynamical equations, is feasible at all (Haff, 1983; Kadanoff, 1999; Gollub, 2003; Depken et al., 2006; Goldenberg

et al., 2006; Meier et al., 2007; Rycroft et al., 2009; Andreotti et al., 2013; Zheng and Yu, 2014).

The recent contribution of Jop et al. (2006) find its place in this ongoing debate. They proposed a constitutive equation (hereinafter the *JFP model*), for the stress tensor of granular media, relying on dimensional arguments. Such a constitutive equation has been tested on some simple geometries and/or flow conditions, showing a remarkable agreement with experiments (Baran et al., 2006; Forterre, 2006; Lagr e et al., 2011; Staron et al., 2012). However, to our best knowledge, it has not yet been tested in a fully 3D complex geometry.

1.1 Work motivation

The aim of this thesis is to apply the JFP model to the fully 3D complex flow situation represented by the flow of dry monodisperse grains inside an horizontal half-filled cylinder rotating about its axis, the so called *rotating drum* problem, which is considered a benchmark for dense granular flow.

The thesis is organized as follows: a review of the literature is given in Chapter 2 along with a description of the JFP model; the model equations and their solutions are discussed in Chapter 3; in Chapter 4 some novel results will be presented and discussed; finally, in Chapter 5, some conclusions are drawn, and future perspectives are outlined.

2.1 Generalities on rotating cylinders

Using the words of Seiden and Thomas (2011), “*The rotating drum is particularly associated with the study of dense granular flows*”. Rotating cylinders are hollow cylindrical containers filled (partially or totally) with grains and put in rotation about their axes. The system is subjected to non-trivial dynamics caused by a gravity-driven non-homogeneous flow (GDR MiDi, 2004), and displays a wide variety of possible behaviors and flow configurations (Seiden and Thomas, 2011).

This configuration is frequently used as model for many problems, here included mixing and/or segregation of grains, suspension or emulsion dynamics. The dynamics in these cases can be very complex and the systems present peculiar segregation patterns (Metcalf and Shattuck, 1996; Ottino and Khakhar, 2000). Although the analysis of such dynamics is beyond the scope of this work, it is apparent that a robust and reliable description of the “simple” flow dynamics inside rotating cylinders would eventually be quite

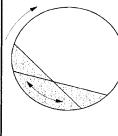
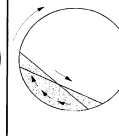
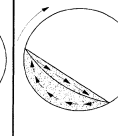
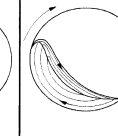
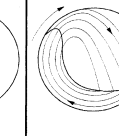
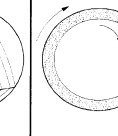
Basic form	Slipping motion		Cascading ("tumbling") motion			Cataracting motion	
Subtype	Sliding	Surging	Slumping	Rolling	Cascading	Cataracting	Centrifuging
Schematic							
Physical process	Slipping		Mixing			Crushing	Centrifuging
Froude number Fr [-]	$0 < Fr < 10^{-4}$		$10^{-5} < Fr < 10^{-3}$	$10^{-4} < Fr < 10^{-2}$	$10^{-3} < Fr < 10^{-1}$	$0.1 < Fr < 1$	$Fr \geq 1$
Filling degree f [-]	$f < 0.1$	$f > 0.1$	$f < 0.1$	$f > 0.1$		$f > 0.2$	
Wall friction coeff. μ_w [-]	$\mu_w < \mu_{w,c}$	$\mu_w \geq \mu_{w,c}$	$\mu_w > \mu_{w,c}$			$\mu_w > \mu_{w,c}$	
Application	no use		Rotary kilns and reactors; rotary dryers and coolers; mixing drums			Ball mills	no use

Figure 2.1: Flow configurations table by Mellmann (2001).

beneficial. In this review of the literature about granular flows inside rotating cylinder only works regarding the flow characterization will be reported, leaving aside the vast literature on granular segregation and mixing happening in rotating cylinder (see Ottino and Khakhar, 2000, for a review of the literature on those topics).

The rotating drum problem has its origin in the industrial problems involved in processing granular materials: drying/humidifying, mixing, heating/cooling or calcining processes make often use of rotating cylinders in order to keep the material in motion and to process it in a uniform manner. It is then important to model such flows, and phenomenological models began soon to be published (Vàhl and Kingma, 1952; Kramers and Croockewit, 1952; Franklin and Johanson, 1955; Scott et al., 2008).

Great effort to classify the flow behavior of granular materials in rotating cylinders was spent by Henein et al. (1983), who proposed the use of "Bed Behavior Diagrams" to conveniently delineate the different flow behaviors.

The most thorough systematization of the possible granular flow configurations was proposed by Mellmann (2001), who identified several flow regimes, shown in Figure 2.1, and the transitions among them by means of model calculations.

Mellmann identified three basic form of the flow, namely the *slipping motion*, at low filling and low friction, where the grains do not flow and move as a bulk; the *cascading motion*, at medium rotational velocities, characterized by the onset of a liquid-like flow; and the *cataracting motion*, when the centrifugal acceleration is comparable with gravity.

The slipping motion occurs when the friction between the cylinder walls and the grains is sufficiently low. When walls are very smooth sliding may be observed, which is characterized by a bed constantly sliding on the wall. With increasing wall friction, sliding turns into surging. This type of motion is characterized by periodic alternation between adhesive and kinetic friction of the bed on the wall. Those regimes does not involve a proper flow of the material but a bulk motion of the entire bed.

When the friction increases, the granular bed starts to flow. When the rotation velocity are low, the slumping flow may occur. This flow consist in a series of successive distinct avalanches. As the rotational speed increases, a transition to rolling flow takes place, and the discrete sequence of avalanches evolves into a single continuous motion in the upper part of the bed. As the rotational speed further increases, the bed surface begins to arch and cascading sets in.

At high rotational velocities the typical arch of the cascading regimes became so pronounced that it eventually breaks up and particles are thrown

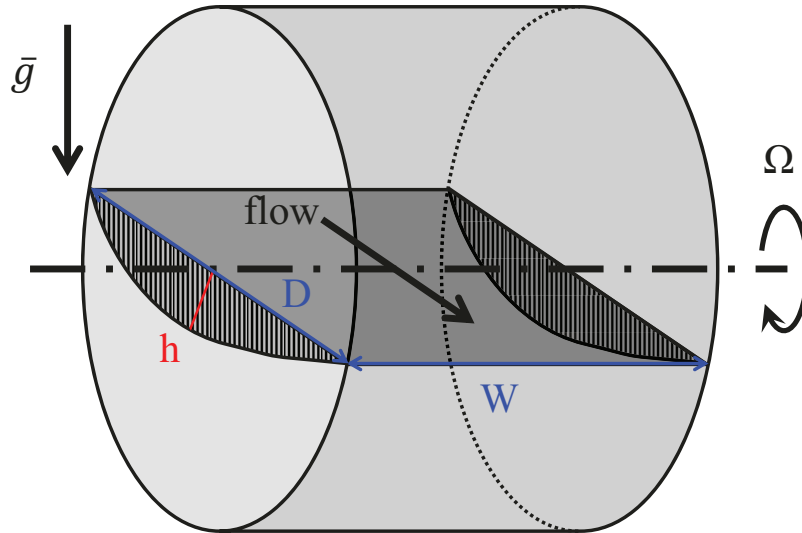


Figure 2.2: Sketch of the geometry and of the flow. The shaded area is the flowing layer, h its depth; D and W are the diameter and the width of the cylinder, Ω the rotation rate.

off into the free space of the cylinder. This regime is called cataracting. At extremely high rotational velocities centrifuging sets in, and the granular bed coats the whole inner surface of the cylinder and moves attached to it as a solid.

In this thesis only the rolling and the cascading regimes will be considered. Those non-uniform flows are characterized by the co-existence of a fixed bed that rigidly rotates, following the cylinder, and a continuously fed flowing layer (the shaded area in Figure 2.2), just below the free surface. Since only half-filled cylinders will be considered, the relevant quantities for the description of the flow are: the diameter D and the width W of the cylinder, the rotation rate Ω , and the physical properties of the grains, like their mean diameter d_p and some other, used to describe their rheology, which will be

discussed in Section 2.5. These parameters are usually arranged in three dimensionless groups: the *Froude number* Fr , which is the ratio between the inertia and the gravity, the *diameter ratio* D/d_p and the *aspect ratio* AR .

$$Fr = \frac{(\Omega R)^2}{gR} = \frac{\Omega^2 R}{g}, \quad \frac{D}{d_p}, \quad AR = \frac{W}{D}. \quad (2.1)$$

2.2 Review of experimental literature

Since grains are opaque, the interior of the flow can not be investigated with optical methods. On one hand this makes the study of granular material experimentally challenging, requiring complex procedures and apparatus. On the other hand it pushed the past works toward simple approaches, like measuring quantities directly available to naked eyes (or to fast cameras), such as, e.g., the flow near a transparent end wall, or the free surface of the flowing grains. The observable available in the latter examples of “direct measurements” are the velocity profiles along the depth of the granular phase and on its free surface, the depth of the flowing layer (h in Figure 2.2), the dynamic angle θ (i.e. the angle between the free surface and the horizontal plane), and the shape of the free surface. Such measurements are usually performed in very narrow cylinders (quasi-2D cylinders), in order to avoid flow in the axial direction.

In order to investigate the flow inside the material a non-invasive experiment has to be devised. Two approaches have been used in this sense: one relies on the use of Magnetic Resonance Imaging (MRI) techniques (Nakagawa et al., 1993), which allows to capture a snapshot of the whole flow field;

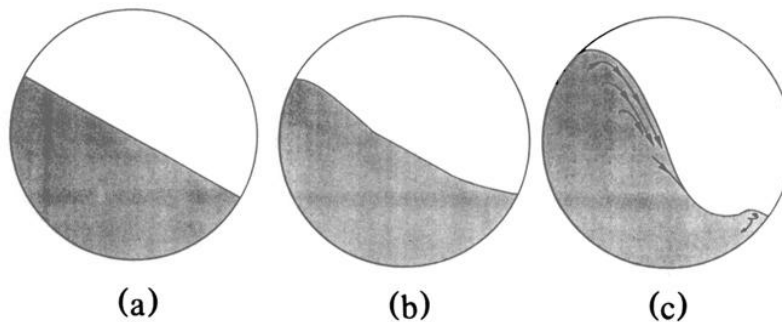


Figure 2.3: Sketch of the free-surface profile. From Rajchenbach (1990).

another relies on the Positron Emission Particle Tracking (PEPT) (Parker et al., 1997, 2005), which allows the tracking of individual trajectories. Those are very complex experiments and their space and time resolutions are quite lower than those pertaining to direct measurements ($\sim 0.3s$ e $\sim 0.8mm$ for the MRI (Nakagawa et al., 1993), $\sim 1/20s$ ($1/250s$) and $\sim 2mm$ ($5mm$) for slow (fast) particles for PEPT (Parker et al., 1997)). Nevertheless, such experiments allow for the inspection of the *inside* of the flow far from end walls, while the quasi-2D approaches cannot avoid wall effects. We believe this to be a crucial point: even if it is commonly accepted that there is a strong influence of the lateral wall on the flow (Pignatel et al., 2012; Jop et al., 2005; Pohlman et al., 2006a; Chen et al., 2008; Dury et al., 1998; Maneval et al., 2005), most of the experiments are in fact performed in the worst condition, i.e. by looking at grains near a wall.

Rajchenbach (1990) performed one of the first experiments on granular flow inside rotating cylinders from a pure-research (rather than technological) point of view, prompted by previous works on granular avalanches (e.g. Jaeger et al., 1989). He studied the transition between slumping and rolling

(i.e. between separate avalanches and continuous flow) in a cylinder with $D = 19\text{cm}$ half-filled with particles having diameter $d_p = 0.3\text{mm}$ and observed the gradual arching of the free surface, which eventually attained a pronounced S -shape (see Figure 2.3). He linked this behavior to the interplay of the centrifugal force and the gravity: while the former tends to maintain the particles attached to the wall, the latter pushes them down into the flowing layer; the result is that beyond a certain rotation rate Ω particles are launched into parabolic trajectories. He also observed a quadratic dependence of the rescaled dynamic angle on the angular velocity $\theta - \theta_s \propto \Omega^2$, θ_s being the angle of repose.

Orpe and Khakhar (2001) considered quasi-2D cylinders filled with three different grains (steel, glass and sand) and studied the effect of the Froude number Fr and d_p/R on θ , h and the shape of the free surface. They found that h/R increases with increasing Fr and d_p/R . The dynamic angle θ showed a non-linear increase with the angular velocity Ω , but it did not scale with Fr or d_p/R . The free surfaces at the wall for the various materials were found to collapse when Fr and d_p/R are held constant. The authors also compared their results with the models by Elperin and Vikhansky (1998), which showed good agreement for low Fr , and Khakhar et al. (1997), who was in agreement with the data over the entire range of Fr .

Jain et al. (2002) studied the flow of glass particles inside quasi-2D rotating cylinders, obtaining a linear velocity profiles in the flowing layer with an exponential tail in the rigidly rotating part. A creep motion in jammed grains has also been observed in heap flows by Komatsu et al. (2001). Jain et al. (2004) also studied the influence of the interstitial fluid.

Alexander et al. (2002) studied the surface flow of glass beads with $d_p = 1.6\text{mm}$ in rotating cylinder with the same width $W = 30\text{cm}$ and different diameters. They found two different scalings, for high and low velocities, for the streamwise velocity on the free-surface at the center of the cylinder, but they did not report any dependence on the aspect ratio.

Taberlet et al. (2003) observed experimentally what they called “super-stable granular heap”: when the flow rate is sufficiently high and the heap sufficiently narrow, the grains flow at considerably higher angles than the angle of repose. They suggested a linear scaling of the “big” dynamic angle with the ratio between the flow thickness and the width of the heap h/W .

A review of experimental data obtained by investigating the flow close to the lateral wall can be found in GDR MiDi (2004) and Pignatel et al. (2012). GDR MiDi (2004) reviewed the main experimental results for each of the six configurations in which granular flows are studied. With regards to the rotating cylinder problem, the French group analyzed data collected from Orpe and Khakhar (2001); Bonamy et al. (2002b); Félix et al. (2007) and from some private communications. They analyzed the rotating drum and the heap problems in the same section, since both of them present a flowing layer on top of a fixed bed, and found that the parameter giving the best scaling was the dimensionless 2D flow rate Q^* , which can be expressed in terms of our dimensionless parameters as (Pignatel et al., 2012):

$$Q^* = \frac{Q}{d_p \sqrt{d_p g}} = \frac{\frac{1}{2} \Omega R^2}{d_p \sqrt{d_p g}} = \frac{\sqrt{2}}{8} Fr^{\frac{1}{2}} \left(\frac{D}{d_p} \right)^{\frac{3}{2}}$$

where $Q = \frac{1}{2} \Omega R^2$ is the planar flow rate of material brought up by the rigid

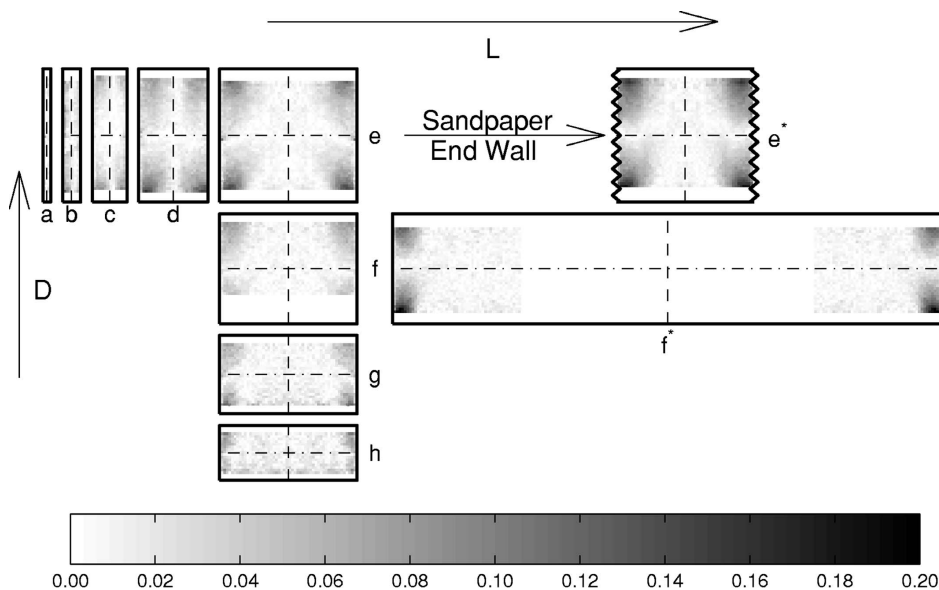


Figure 2.4: Density plots of the axial velocity magnitude on the free-surface of the flowing layer for various AR . The cylinders are drawn to scale. Their L is the width of the cylinder, here called W . From Pohlman et al. (2006a).

rotation in half-filled cylinders.

They found that the velocity close to the wall of quasi-2D cylinders is linear with the depth and that the dimensionless thickness of the flowing layer h/d_p scales with $\sqrt{Q^*}$. This is what one would obtain by hypothesizing a constant shear rate in the flowing layer, consistently with the linear velocity profile, and solving the flux balance for the thickness h . This seems to be a quite robust result, but it comes from near-wall data; in Chapter 4 we shall discuss it further. GDR MiDi also noted a decrease in the dynamic angle θ with increasing cylinder width, i.e. with AR , even if the aspect ratio was not the only different parameter from one dataset to another.

Pohlman et al. (2006b) analyzed the effect of the particle surface roughness on the flow inside quasi-2D cylinders, finding an increasing of the dy-

dynamic angle θ with the roughness. Pohlman et al. (2006a) studied the surface velocity on the free surface of 3D cylinders. To get rid of the optical distortion of the lateral wall, the authors cut out a quarter of the cylinder and set the camera as to film through the opening. This meant, however, that they could acquire data only on one quarter of one whole cycle. They measured the axial flow in dependence of the diameter and the width of the cylinders and presented contour and density maps of the axial velocity, the latter shown in Figure 2.4. The axial flow is directed toward the center in the upper part of the free surface and toward the end walls in its lower part. They observed for the first time a velocity near the wall $\sim 20\%$ *higher* than that at the center of wide cylinders, even if the particles closer to the wall were slower due to friction (see Figure 2.5). Looking at the contours of axial velocity the authors could deduce the range of wall effects as the distance at which the axial flow is negligible, finding it to be of the order of the diameter of the cylinder. This is in strong disagreement with the accepted idea that the range of wall effects is of the order of few beads diameters (Courrech du Pont et al., 2003; GDR MiDi, 2004; Boltenhagen, 1999; Grasselli and Herrmann, 1997), but in qualitative agreement with Dury et al. (1998) who found that, for $D/d_p > 15$, the range of the wall effects is $0.14D$ and with Chou and Lee (2008), who reported wall effect even $57d_p$ away from it.

Orpe and Khakhar (2007) studied the velocity profiles in a quasi-2D cylinder. They always found a linear profile in the flowing layer which decay exponentially in the rigidly rotating zone with a characteristic length of decay of $\sim 4d_p$.

Chou and Lee (2008) analyzed the effects of the filling degree, aspect ratio

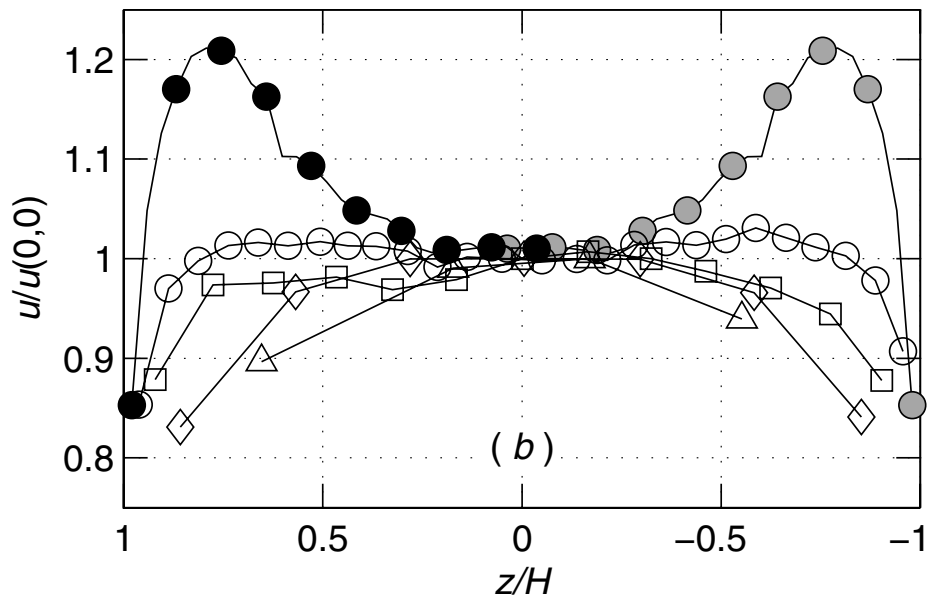


Figure 2.5: The streamwise surface velocity as a function of the axial position. From Pohlman et al. (2006a).

and angular velocity of the cylinder on the velocity of the grains. They found a good scaling with the dimensionless flow rate Q^* . They also registered an error in the mass balance between the grains brought up by the rotation and those flowing down at the wall; in particular, they found that the former is *less* than the latter. Coupling this evidence with the observation of a lower velocity in the center of a cylinder with respect to that near the wall (Maneval et al., 2005; Pohlman et al., 2006a), one might explained this with an underestimation of the flow thickness far from the wall. This is an indirect indication of the fact that h should increase going from the wall toward the center of a cylinder.

Félix et al. (2007) reported a monotonically increasing scaling of the dynamic angle and the flow depth with the rotational velocity; they found,

however, a wide exponent range for the power law dependency of the flow depth on the rotational velocity, with values going from 0.17 to 0.68, depending on the ratio D/d_p . The angle is also found to increase with decreasing width, even if an appropriate parameter to collapse the data is not proposed. It has to be noticed that the authors did not consider the width of the cylinder as an important parameter, so they simply reported its value, without controlling it thoroughly.

Pignatel et al. (2012) analyzed a collection of data from literature on quasi-2D cylinders (Orpe and Khakhar, 2001; Félix et al., 2007; Jain et al., 2004; Khakhar et al., 1997; Jain et al., 2002). They registered a scatter of the power law index of h/d_p versus Fr as well, but found a better scaling with $\sqrt{Q^*}$. The authors could not explain their data with the JFP model, probably due to the poor estimates of its parameters or because of the very narrow cylinders ($W < 22d_p$).

There are few works dealing with the measurements of flow properties *at the center* of a wide cylinder. As already said, this is allowed by MRI and PEPT technologies, but it comes with a price in terms of spacial/temporal maximum resolution. Nonetheless those techniques are currently the only way to look at the behaviors of dry grains deep into the material.

Nakagawa et al. (1993) conducted the first experiment on dry granular materials with a non-invasive technique. He used the Magnetic Resonance Imaging (MRI) to study the flow of mustard seeds inside a wide rotating cylinder. The most important result of this work is the earliest experimental measurement of the concentration profile inside the flowing layer. The authors reported density plot of both velocity and concentration in the center

of the drum. It's clearly visible that the flowing layer has a sensibly lower grain concentration than the rigidly rotating part. The same authors also applied MRI to segregation (Nakagawa, 1994; Nakagawa et al., 1997).

MRI experiment allows comparison between the center and the wall of rotating cylinder. Yamane et al. (1998) and Dury et al. (1998) focused on the differences between the dynamic angles at the center θ_c and the wall θ_w of a cylinder filled with mustard seeds. They both found that the dynamic angle was $\sim 5^\circ$ higher near to the wall than at the center of the cylinder at all the angular velocities explored, with an exponential decay of θ_w in $\sim 0.14D$. This is the first time that the wall effect is reported to scale with a macroscopic scale (D) instead of a microscopic one (d_p).

Maneval et al. (2005) and Sanfratello et al. (2006) focused on the velocity profiles differences between center and wall. Both reported a velocity profile observing the following equation in the flowing layer at both center and wall:

$$v(r) = \begin{cases} -v_{top} \left(1 - \frac{r}{h}\right)^2 + \Omega r & r < h \\ \Omega r & h < r < R \end{cases}$$

where v_{top} is the maximum velocity, on top of the free surface, h the depth of the flowing layer, Ω the angular velocity and R the radius of the cylinder. Maneval et al. (2005) reported an higher velocity at the center with respect to that at the wall (see Figure 2.6(a)). Sanfratello et al. (2006) found the same profile at higher angular velocities, provided that the free surface is kept flat by a paddle to avoid the arching. They suggested that a parabolic velocity profile might be a fundamental properties of granular flows.

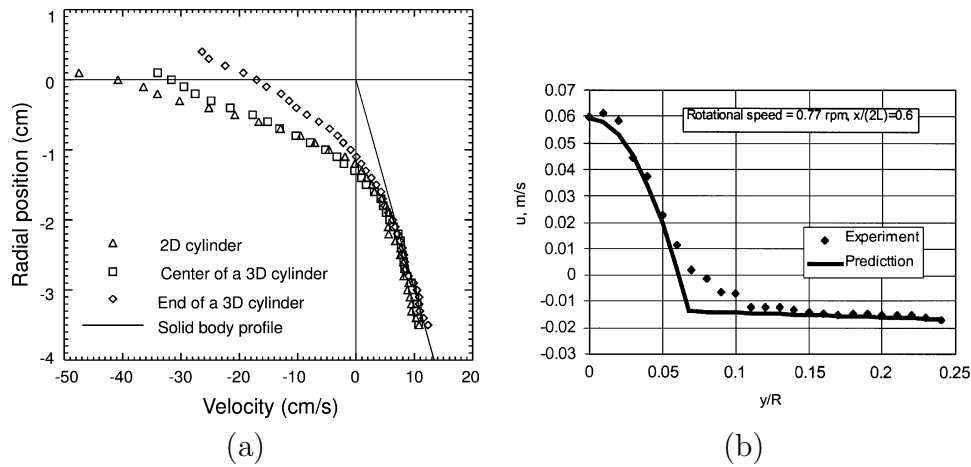


Figure 2.6: Velocity profiles measured with MRI (Maneval et al., 2005) (a) and PEPT (Ding et al., 2001) (b).

Another technique to study the flow inside an opaque material is the PEPT. Parker et al. (1997) performed the first experiment with such technique in rotating cylinders. They used glass spheres of various diameter in a long cylinder at 33% filling degree, obtaining the velocity field at its center. The authors reported a non-linear velocity profiles in the flowing layer and the distributions of angular velocity in the fixed bed. Some of the velocity distributions, beside showing the existence of some slip between grains and cylinder, display two peaks and the authors suggest that they might correspond to distinct layer of beads rolling over each other.

Ding et al. (2001) studied the velocity of glass beads in the rolling flow regime with a filling degree $< 50\%$ and they focused on scaling parameters. The velocity clearly show a more than linear profile in the flowing layer (see Figure 2.6(b)), confirming the first observation of Parker et al. (1997).

2.3 Review of numerical literature

The most commonly adopted numerical approach to study granular materials is the Discrete Element Method (DEM) (Zhu et al., 2007): the granular material is modeled as an assembly of rigid particles and the interactions among them are explicitly considered. This technique has the advantage to reflect the discrete nature of the medium and to access the very local details of the flow. Nevertheless its major drawback is the relatively limited number of particles which can be effectively handled: as an example, we mention a very recent DEM calculation on a system made up of more than one million particles (Longmore et al., 2013), which is an estimate of the number of grains contained in a teaspoon full of sugar; a small lab cylinder with a diameter of 20cm and a width of 40cm , half-filled with grains having a diameter of 0.5mm and a void fraction of 0.5, would contain *48 million* particles. Conversely, a continuum approach would overcome this limit at the price of losing the fine grain-scale details of the flow.

While many numerical studies on rotating cylinders uses the DEM approach, only two attempts have been done to describe this flow as a continuum: Demagh et al. (2012) and Huang et al. (2013) both solved the Eulerian–Eulerian formulation of the balance equations coupled with the kinetic theory for dense flows (Vun et al., 2010). Both of them used a Finite Volume Method for solving the model equations.

Demagh et al. (2012) focused on very low filling degree in order to identify the scale-up rules for an industrial cement kiln.

Huang et al. (2013) performed 2D and 3D simulations of the segrega-

tion inside rotating cylinders. They estimated the granular viscosity, to be plugged into the final simulations, by comparing the dynamic angle obtained in simulations with the experimental one. They found discrepancies between 2D and 3D simulations and linked them to the higher number of degrees of freedom in the latter case. They reported a qualitative agreement between the radial and axial segregation patterns and the experiments.

2.3.1 Discrete approaches

DEM simulations are particularly well-suited to study the influence of grain interactions on macroscopic behaviors. There are two main approaches in DEM simulations: soft-particle and hard-particle. The former method has been developed by Cundall and Strack (1979) and was the first granular dynamics simulation technique published in literature. It basically consists in solving the Newton's laws of motion for each particle in the system taking into account the interactions among them. The peculiarity of this method is that the particles are allowed to undergo tiny deformations, and these deformations are used to calculate the elastic, plastic and frictional forces between grains. The soft-particle method is able to handle multiple contacts at the same time: this is crucial when dealing with dense flow, since particles are always in contact with many neighbors. The hard-particle method, instead, does not model forces by means of particle deformation (hence the name of the methods) but by instantaneously collisions handled one at time: this make the method most useful for rapid collisional granular flows (Zhu et al., 2007).

DEM simulations have been extensively used to study the whole range of grain-related phenomena, such as particle packing, transport properties, heaping/piling process, hopper flow, mixing and granulation (for a review of DEM results for particulate system see Zhu et al., 2007, 2008).

Pöschel and Buchholtz (1995) performed 2D DEM simulations with both disks and non-circular objects with a soft-particle approach. They recovered some of the feature of the rolling flow regime, e.g. the increase of the dynamic angle with Ω and the typical S -shape of the free surface. Their non-spherical grains, which are made by disks 5 disks connected by springs, also reproduced the stick-slip behavior observed in experiments. Similarly, Buchholtz et al. (1995) studied 2D square grains made by four triangles connected by four elastic beams, confirming that non-spherical grains have better agreement with experiments (e.g. those in Rajchenbach, 1990) than spherical ones.

The first quantitative agreement with experiments came with the work of Ristow (1996). He compared the dynamic angle θ and the surface velocity obtained in 2D contact dynamic simulations with the experiments by Nakagawa et al. (1993). The author then inferred that DEM simulation are appropriate for a detailed study of the granular flow in rotating cylinders.

Yamane et al. (1998) performed the first 3D DEM simulations of rolling and cascading flow. They compared their results with MRI data both at the center and at the wall, finding an excellent agreement for the dynamic angle. They also registered a difference in the shape of the free surface, with the experimental one being flatter than the numerical one.

Yang et al. (2003) studied the microstructure of the granular material inside rotating drum by means of 3D DEM simulations. They found an

excellent agreement with PEPT measurements by Parker et al. (1997) on both dynamic angle and velocity along a line orthogonal to the free surface at the center of the cylinder.

Those early work served mainly to assess the feasibility of DEM simulation as a modeling tool for granular flow inside rotating cylinders.

Renouf et al. (2005) used the Non-Smooth Contact Dynamic Method (Jean, 1999) to study the rheology of granular dense flow. Their 2D simulations quantitatively matched the $\mu(I)$ profiles obtained by Silbert et al. (2001) for granular flow down a rough inclined plane with both 2D and 3D DEM simulations.

Pohlman et al. (2006b) used particle dynamics simulations to verify their experimental result that inter-particle friction plays a role in determining the dynamic angle θ inside a rotating cylinder. They studied several mixture of smooth and rough steel balls, obtaining an increasing θ with increasing volume fraction of rough particles.

Taberlet et al. (2006) numerically studied the S -shape of the free surface. They developed a model which accounts for the effects of the end walls, which appear to be crucial in the determination of the free-surface shape, and proposed a scaling parameter which allows to collapse all the interface profiles.

Chen et al. (2008) studied the 2D velocity profiles on the free surface of wide cylinders numerically. They observed the existence of an axial flow near the walls directed toward the center in the upper part of the flowing layer (upstream), and toward the lateral wall in the lower part of such layer. This work is the numerical equivalent of what Pohlman et al. (2006a) did experi-

mentally. The axial flow increases with the wall friction and with the flowing length (i.e. with the diameter). The axial flow produces higher streamwise velocities, which can be justified with conservation of mass arguments. They also pointed out that such a flow extends for a distance of $L = 0.5D$ from lateral walls.

Third et al. (2010) performed 3D DEM simulations to study the tangential velocity profiles in rotating cylinders. The authors confirmed the quadratic profile reported by Nakagawa et al. (1997) and reported a slip at the walls that depends on the filling degree of the cylinder. Their simulations also showed that a slip between two layers of grains, i.e. a *shear band*, might occur at low filling levels. This kind of slip is not included in the Mellmann (2001) classification of the flow regimes.

2.4 Review of theoretical literature

Many efforts have been put forward to develop a theory for the description of granular flows. Some authors focused on extending the existing theory for diluted assembly of collisional spheres, the so called kinetic theory (Goldhirsch, 2003), to dense frictional spheres (Haff, 1983; Campbell, 1990; Jenkins and Berzi, 2010; Berzi, 2014). Another part of the scientific literature is devoted to the development of continuum models (Meier et al., 2007) to describe such dense flow. Since the flow is usually limited to few grains on top of a fixed bed, many of those models are based on the assumption of shallow flowing layer, which allows the definition of depth-averaged quantities. For a derivation of the depth-averaged equations see Andreotti et al. (2013).

The first attempt to link “macroscopic” rheology to “microscopic” mechanics was made by Bagnold (1954) for dispersions of grains in water and by Savage (1979) for dry grains. Savage (1979) proposed a constitutive equation for cohesionless bulk solids under conditions of rapid shear on inclined chutes and channels. The constitutive equation describes a Coulomb material, for which the normal and shear stresses are related, and refers the stresses to the deformation rates in a nonlinear way, in accordance with Bagnold (1954). He could find only a qualitative agreement with his own experiments, maybe because of the presence of friction on the glass side walls of the flow passages, which were not included in the model. The experiments reflected the general trends of the analysis in the shapes of both the velocity profiles and the depth profiles in the inclined chute, and this suggests that the most prominent effects have been included in the proposed constitutive relations.

Savage and Hutter (1989) presented, for the first time, a formal derivation of evolutive shallow-water equations for granular material. They integrated the mass and momentum equations along the depth of the flowing layer, assuming a Mohr–Coulomb internal rheology and a constant Coulomb basal friction law. They integrated the model equations with both an Eulerian and a Lagrangian approach and compared them with results on rockslide motion, obtaining good qualitative and fair quantitative agreement of the propagation of the front and rear margins of the avalanche as well as the evolution of the shape of the depth profile.

Bouchaud et al. (1994) developed a model, referred as *BCRE* from the name of the authors, for the granular avalanche problem based on the dynamical interchange of two populations of grains: immobile, those in the fixed

bed, and rolling, those which participate to the avalanche. The assumption is that the avalanche starts when a sufficiently strong perturbation trigger the event: this include the possibility of an *hysteresis*. The model describes the avalanche as an erosion–deposition process which starts at a *spinodal* angle, higher than the angle of repose, at which the system becomes unstable to an infinitesimal perturbation. They applied the model to the slow slumping regime, i.e. when the time for an avalanche to reach the bottom of the free surface, which is rotation independent, is much less than the time needed to restore the spinodal angle; if those times become comparable the system will enter the rolling regime. In such a way they could estimate the frequency crossover value at which the transition happens for glass beads in a cylinder with $D = 0.1m$, finding a value of $\sim 0.5rpm$.

Boutreux et al. (1998) expanded the *BCRE* model to account for *thick* avalanches: they assume that when an avalanche starts, the depth of the falling layer is χ , where χ is a characteristic mesh size, typically $\chi \approx 5d_p$. Even starting with pretty narrow layers, avalanches rapidly reach much larger thickness and the population of falling grains cannot be considered constant anymore. Aradian et al. (1999) further developed this point including also a non-constant velocity profile in the falling layer. Douady et al. (1999) included in their *BCRE*-like model an explicit dependence of the free-surface shape on the flow condition during an avalanche.

Khakhar et al. (1997) presented a continuum model of a rotating cylinder based on a depth-averaged steady state momentum and mass balance between the flowing layer and the fixed bed on its bottom. The 1D model holds for low angular velocities (i.e. narrow flowing layer) and flat free surfaces.

The shear stress is taken to be a sum of the frictional and the collisional stresses. The latter is calculated using the result of Bagnold (1954) and its magnitude depends on an adjustable parameter, which can be calculated by specifying the physical properties of grains, the operating conditions (filling degree and angular velocity) and the velocity profile function in the flowing layer (the authors did the calculations for a plug flow, a linear profile and a Bagnold (1954) profile). The model predicts the shape of the flowing layer and its average velocity along the free surface.

Elperin and Vikhansky (1998) used a similar approach to develop a model which accounts for the curvature of the free surface. Their model takes into account only the collisional stresses and neglects the frictional stress and assumes a Mohr–Coulomb failure criterion (shear to normal stress ratio equal to a constant friction coefficient). The frictional forces are implemented in the model by two adjustable parameters which depends on the friction inside the flowing layer. Under these simplification the authors calculated analytical solutions for the shapes of both the free surface and the flowing layer and for the depth–averaged velocity along the free surface. Also Zik et al. (1994) proposed a model for the free–surface shape based on the mass balance in the approximation of thin flow.

Makse (1999) underlined the importance of considering a flux–dependent velocity. Using the shear rate as a fitting parameter, they could match the experimental trends by Nakagawa et al. (1993) and Khakhar et al. (1997). The authors argued that *“the predictions based on the common assumption of a constant velocity profile of flowing grains are in error. The profiles predicted by the theory agree with experiments only when a height–averaged*

velocity profile is taken into account”.

Ding et al. (2001) developed a model for describing the rolling flow at the center of a rotating cylinder. The authors proposed a parabolic velocity profile which only depends on the ratio Λ between the positions of the zero-velocity line and of the active/passive interface, arguing that this parameter depends only on the rheology of the material. Under those assumption they derived a shallow-water equation to describe the flowing layer depth profile and the mass exchange between the bed and active and the passive zones. Using this model, the same author described the transition between the rolling and the slumping regimes in a successive work (Ding et al., 2002). They identified the characteristic times needed to have all the grains in the system to flow in the active layer in both regimes: by equating them they could extract the rotation rate of the transition, which depends on the filling degree, on the difference δ between the maximum and a minimum angles in slumping regime, on the time needed by an avalanche to reach the bottom of the flowing layer and on Λ , but not on the diameter of the rotating cylinder (which however is hidden in the avalanche time). Assuming half-filled cylinders, $1^\circ < \delta < 30^\circ$, $0.7 < \Lambda < 0.9$ (Ding et al., 2002) and avalanche time equal to $1s$, the critical rotation rate is between $0.1rpm$ and $1rpm$.

Pohlman et al. (2006c) found that the surface velocity in the midpoint of a 3D tumbler scales linearly with the length of the flowing layer, no matter the geometry of the tumblers (spherical, cylindrical, . . .) or the filling degree. A simple model, which assumes that the axial flow is negligible, allows the estimation of the depth-averaged velocity in the flowing layer and predicts this scaling.

Jenkins and Berzi (2010) extend the kinetic theory for dense flows of identical, nearly elastic, frictionless spheres (Jenkins, 2007) to identical, very dissipative, frictional spheres. The parameter of the model have been extracted from inclined plane experiments and the results of the model have been tested against experimental data on confined heaps. The same authors further extended their model to include a dilute collisional layer on top of the dense flowing one (Berzi and Jenkins, 2011). The proposed model accounts for wall effects by including a wall friction factor, as already done by Taberlet et al. (2003) and Jop et al. (2005). The inclusion of a dilute layer allow them to quantitatively model the data from Félix et al. (2007) on rotating cylinders and to verify the dependence of the dynamic angle on the width of the channel experimentally observed by Courrech du Pont et al. (2003). Berzi and Jenkins (2011) concluded by observing that a local rheology can be applied only when the whole flow is dense, i.e. when the dilute layer thickness is negligible.

2.5 JFP model

Recently Jop et al. (2006) have proposed a continuum description of dense granular flows, based on the local rheology approach proposed by GDR MiDi (2004). The proposed constitutive law, which shares some similarities with classical constitutive equation of visco-plastic fluids such as Bingham fluids, allows a Finite Element Method (FEM) or a Finite Volume Method (FVM) numerical simulation of granular flows.

GDR MiDi (2004) proposed “*a rheology for which stresses and shear rate at a given location in the flow are related through a one to one relation*” based on dimensional analysis of pure shear flow. They argued that, since there is no influence of the microscopic timescales (those at which the dissipation occurs) on the flow properties, there are only two dimensionless parameter that can be defined, the effective friction coefficient:

$$\mu_{eff} = \frac{\tau}{p} \quad (2.2)$$

and the inertial number:

$$I = \frac{\dot{\gamma} d_p}{\sqrt{\frac{p}{\rho_p}}}. \quad (2.3)$$

The inertial number I can be interpreted as the ratio between two time-scales: the flow timescale $1/\dot{\gamma}$ and a confinement timescale $d_p \sqrt{\rho_p/p}$, which is the time needed by a grain to fall from the top of another grain to its level. In this picture, the volume fraction ϕ of the grains must be a variable of the inertial number. They further argued that, in order for a local rheology to exist, there must be a unique relation between μ_{eff} and I .

Jop et al. (2005) extended previous studies on inclined planes (Pouliquen, 1999; Pouliquen and Forterre, 2002) to the heap case with rough side walls. They proposed an equation for the basal friction coefficient μ_b (i.e. the friction coefficient at the interface between the flowing layer and the rough bottom surface) extending the expression for the dynamics friction coefficient

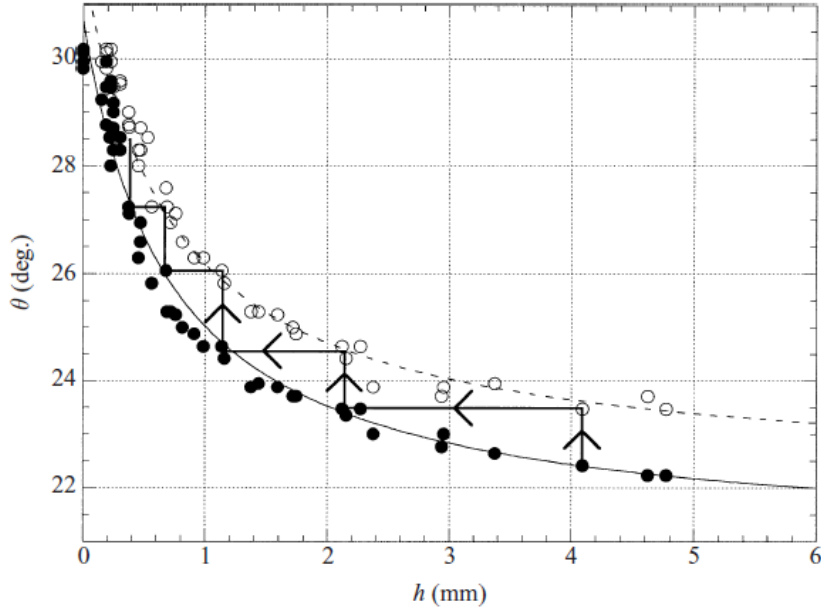


Figure 2.7: Variation of the starting (\circ) and the stopping (\bullet) angles as a function of the thickness h . The arrows indicate the way they are measured: starting with a uniform layer h , θ is increased up to the point where an avalanche occurs. After the avalanche, h has a lower value, θ is increased again and so on. In the $(h; \theta)$ plane, the system oscillate between the starting and stopping curves. Figure 3 in Pouliquen and Forterre (2002).

(see eq. (4) in Pouliquen, 1999):

$$\mu_b(\bar{u}, h) = \mu_s + \frac{\mu_2 - \mu_s}{\frac{h\sqrt{gh}\beta}{\bar{v}d_pL_0} + 1} \quad (2.4)$$

where \bar{v}/h is an average shear rate in the flowing layer and μ_s , μ_2 , L_0 and β are material parameters that can be obtained from experiments on inclined planes. Invoking the rheological relation proposed by GDR MiDi (2004) they

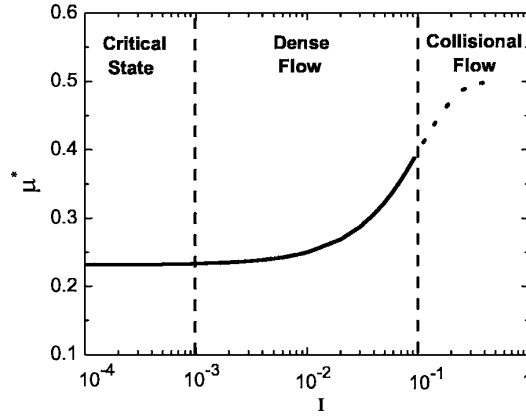


Figure 2.8: Diagram of the granular flow regimes. Figure 17 in da Cruz et al. (2005)

finally ended up with this expression for the friction coefficient $\mu = \mu(I)$:

$$\frac{\tau}{p} = \mu(I) = \mu_s + \frac{\mu_2 - \mu_s}{\frac{I_0}{I} + 1}. \quad (2.5)$$

Granular flow on inclines is known to start at an angle higher than that at which it stops: those angles depends on the thickness of the flowing layer (see Figure 2.7). Equation (2.4), and then Equation (2.5) as well, comes from the fact that the dimensionless velocity scales with the ratio $h/h_{stop}(\theta)$. The material parameter μ_s , μ_2 and I_0 can be obtained from the function $h_{stop}(\theta)$. Using Equation (2.5) with parameter values from different experiments and including the wall friction, Jop et al. (2005) could quantitatively model the flow in a confined granular heap and verify the “*crucial role of sidewalls*”, as they state in the title of their article.

da Cruz et al. (2005) numerically confirmed the validity of the model by means of DEM simulations. They numerically simulated a shear cell by imposing the velocity of the upper plate and the (constant) pressure acting

on it. They confirmed that in the limit of rigid grains the shear state is solely determined by the inertial number: for $I \lesssim 10^{-3}$ the system is in the critical state, i.e. a state of incipient motion, very close to yielding, where the authors observed an intermittent flow; for $10^{-3} \lesssim I \lesssim 10^{-1}$ the system is in the dense flow state, which is of interest here; for $I \gtrsim 10^{-1}$ the system enters the collisional state and the material starts acting like a gas (see Figure 2.8). They also confirm the two functions $\mu = \mu(I)$ and $\phi = \phi(I)$:

$$\phi(I) = \phi_{max} + (\phi_{min} - \phi_{max}) I. \quad (2.6)$$

The former, in particular, is reported to be dependent on the grain friction factor, i.e. on a “microscopic” (sub-grain) quantity, as observed by GDR MiDi (2004): particles with different roughness will have a different $\mu(I)$ curve.

Finally, Jop et al. (2006) proposed a 3D generalization of the 1D constitutive law, which explicitly relies on the assumption that *the (small) variation of the solid volume fraction can be neglected*, i.e. $\phi = \text{constant}$. The granular material, in whatever flow configuration, can be described as a continuum fluid having a stress tensor $\boldsymbol{\sigma}$ given by:

$$\boldsymbol{\sigma} = -p\mathbf{I} + \boldsymbol{\tau} \quad (2.7)$$

$$\boldsymbol{\tau} = 2\eta_{grain}(II_{\mathbf{D}}, p) \mathbf{D} \quad (2.8)$$

$$\eta_{grain}(II_{\mathbf{D}}, p) = \mu(I) \frac{p}{II_{\mathbf{D}}} \quad (2.9)$$

where \mathbf{D} is the rate of deformation tensor, i.e. the symmetric part of the

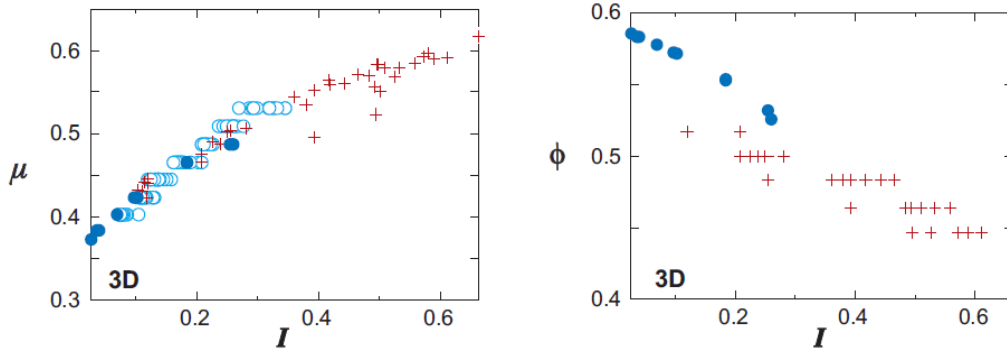


Figure 2.9: Friction coefficient and volume fraction as a function of the inertial number for 3D flows. Open circles represent inclined-plane experiments, where $\mu(I)$ is derived from measurements of depth-averaged velocities at different inclinations and thicknesses (GDR MiDi, 2004; Pouliquen, 1999); filled circles represent inclined-plane simulations (Baran et al., 2006); and crosses represent plane-shear experiments (material II, sample A), in which normal stress and volume fraction measurements were obtained in 3D annular shear cells (Savage, 1984).

velocity gradient $\nabla \mathbf{u}$, and $II_{\mathbf{D}}$ is the second invariant of \mathbf{D} , which is a generalized shear rate (hereinafter we will frequently abuse this notation and write $\dot{\gamma}$ instead of $II_{\mathbf{D}}$). This model is known as JFP model, after the names of the authors who first proposed it (Jop, Forterre and Pouliquen). In this framework the pressure is considered *isotropic* and the shear stress $\boldsymbol{\tau}$ and the rate-of-strain tensor \mathbf{D} are co-linear, i.e. are proportional to each other by the scalar quantity $\eta_{grain}(\dot{\gamma}, p)$. The authors used this model to solve the flow on a confined heap with a finite difference scheme, obtaining excellent quantitative predictions for the free-surface velocity and the lower boundary of the flowing layer for various flow rates and heap widths. The model was shown to poorly describe the flow in the limit of a quasi-2D geometry, i.e. when the heap is $16.5d_p$ wide, as one would expect when the discrete nature of the medium challenges the “continuum” approach.

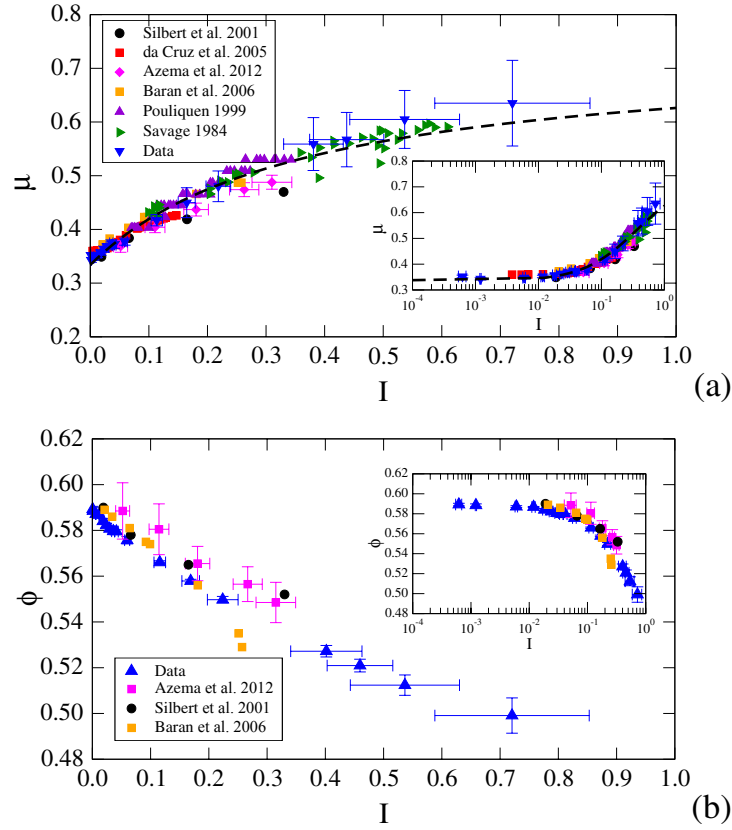


Figure 2.10: Effective friction coefficient (a) and packing fraction (b) as a function of I . Data from (Silbert et al., 2001; da Cruz et al., 2005; Azéma et al., 2012; Baran et al., 2006; Pouliquen, 1999; Savage, 1984), figures from Azéma and Radjai (2014) (references in the legends has been changed to reflect those of the current work).

It should be noticed that the viscosity goes to infinity as $\dot{\gamma}$ tends to zero, like it happens for visco-plastic fluids. In the limit of $II_{\mathcal{D}} \rightarrow 0$ it is possible to show that the above equations reduce to a yield criterion and that the materials flow only if:

$$II_{\tau} > \mu(I)p, \quad (2.10)$$

where II_{τ} is the second invariant of the viscous stress tensor τ .

Figure 2.9 shows experimental and numerical data on friction factor and

volume fraction as a function of the inertial number I . It should be noticed that, comparing Figure 2.9 and Figure 2.8, granular material in the dense flow regime can explore only the initial part of both the diagram in Figure 2.9 (and then the approximation $\phi \approx \text{constant}$ should hold). A more recent collection of those data is shown in Figure 2.10; the insets display the constant values of both μ and ϕ in semi-log plots, evidencing the critical state and the transition to the flow state (see Figure 2.8).

Admittedly, the constitutive law expressed by equations (2.7)–(2.9) still rests on an empirical ground (Jop et al., 2005). Nonetheless, it has been proved to accurately describe many experimental data (Pouliquen et al., 2006).

Forterre (2006) used the 3D JFP model to perform a linear stability analysis of granular flows down inclined planes. He was able to quantitatively reproduce the experiments by Forterre and Pouliquen (2003), in particular the cut-off frequency of the instability (i.e. the frequency above which short wavelengths were stabilized) which could not be reproduced by previous depth-averaged approaches. Their model contains an adjustable parameter responsible for the damping of the short wavelengths. Gray and Edwards (2014) incorporated the JFP model into a depth-averaged granular avalanche model without any fitting parameter, showing an excellent agreement with the results of Forterre and Pouliquen (2003). Very recently such a model has been used by the same authors together with the expressions for the friction coefficients given by Pouliquen and Forterre (2002) (equation (2.4)): it quantitatively predicted the erosion-deposition wave flow of carborundum particles that flow down a rough inclined chute covered with a static erodible

layer of the same grains (Edwards and Gray, 2015). Such flow is made of a series of steadily traveling waves which erode the static layer of particles in front of them and deposit grains behind them, to form a layer that is again stationary.

Lagrée et al. (2011) implemented the JFP model in an incompressible FVM solver and studied the collapse of a column of granular material using the *Volume of Fluid* approach (see Section 3.2 for a detailed explanation of such model). The granular column collapse is another complex situation, with a non-uniform and fully transient flow taking place. Their 2D simulation were able to catch the transient evolution observed with 2D contact dynamic discrete simulations. Another complex flow was tackled by Staron et al. (2012) and Staron et al. (2014). They used the same software of Lagrée et al. (2011) to study the discharge of a silo with 2D continuum simulations. The results are in qualitative agreement with contact dynamic simulations.

2D contact dynamic simulations have also been used by Cortet et al. (2009) to check two fundamental statements at the base of the JFP model: (I) the proportionality between the second invariants of the stress and rate-of-strain tensors and (II) the alignment among them. They focused on the rotating cylinder problem and concluded that while assertion (I) can be considered valid for the whole flow, statement (II) fails significantly over the whole range of inertial number. They further argued that the misalignment between the two tensor might be an effect of the transient compressibility, which is indeed considered negligible by the 3D generalization made by Jop et al. (2006). In this regard Rycroft et al. (2009) reported that such a non-coaxiality decreases by averaging over progressively larger time windows.

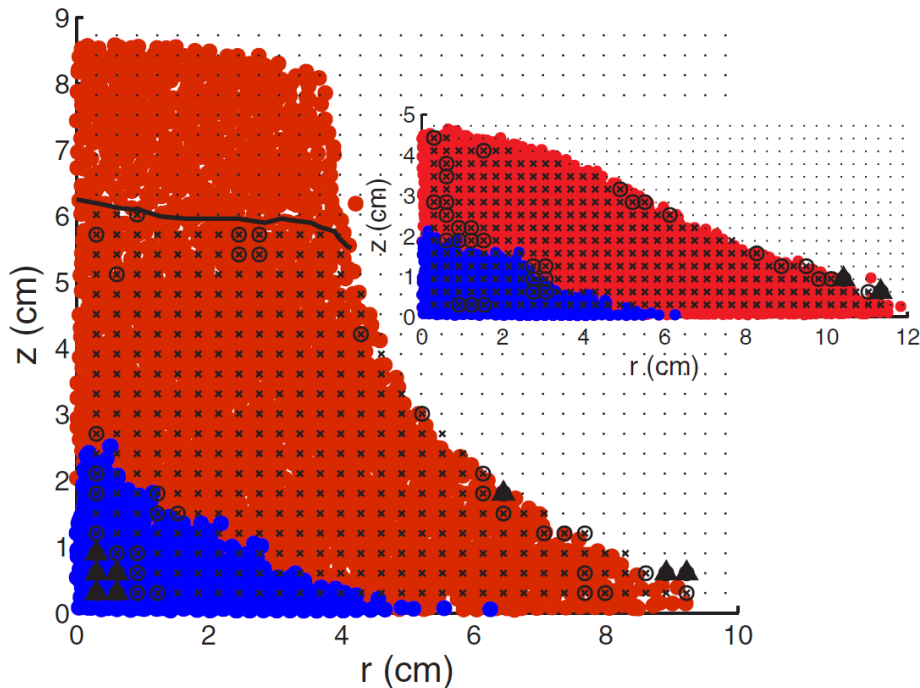


Figure 2.11: Two snapshots of the falling column 3D flow at two different times. Red/blue particles are the flowing/jammed ones, the symbols indicate the degree of misalignment ϕ of the stress and rate-of-strain tensors: $\phi < 5^\circ$ crosses, $5^\circ < \phi < 10^\circ$ crosses with circles, $\phi > 10^\circ$ solid triangles. The black solid line is the interface between the free-falling part and the dense part of the flow. Figure from Lacaze and Kerswell (2009).

Coaxiality is a consequence of material isotropy at the scale of a continuum element (which has a dimension of $\sim 4 \div 5d_p$), so it appears that increasing the time window increases the extent to which the liquid-like material flows approximately like a true continuous fluid.

Lacaze and Kerswell (2009) did a similar analysis on coaxiality in transient 3D soft particle simulations of falling cylindrical piles of granular material, comparing their results with the experiments from Lajeunesse et al. (2004) and Lube et al. (2004). They computed the orientation of the stress

and rate-of-strain tensors during the transient collapse of the column. The analysis was conducted on both the flowing and “jammed” parts of the domain, only excluding the top free-falling zone. A typical snapshot of the flow is shown in Figure 2.11. The author found a general alignment of the two tensor over the entire domain, here included the jammed part (blue in Figure 2.11). They concluded their contribution saying that *“The general applicability of viscoplastic theory found here is, frankly, a surprise given (a) the presence of a large growing static-flowing interface, (b) the proximity of most of the fast flow to the rough bottom boundary and (c) the existence of a large free surface”*.

Chambon et al. (2011) and Minatti and Paris (2015) implemented the JFP model in 2D Smoothed Particle Hydrodynamic codes and were able to quantitatively match the experimental data available for the granular column collapse problem.

Azéma and Radjai (2014) recently connected the “macroscopic” friction law $\mu(I)$ to the contact network and force transmission. They argued that $\mu \simeq \frac{1}{2}(a_c + a_n + a_t)$, where a_c , a_n and a_t are parameters linked to the angular anisotropy of the mean stress on the shear plane (contact anisotropy), of the normal force (force chain anisotropy) and of the tangential force (friction mobilization) respectively. They also found that μ increases with I mainly due to an increasing contact anisotropy a_c . This confirms and gives further physical insight into the dependence of the effective friction coefficient proposed by GDR MiDi (2004) on the inter-particle frictional interactions.

The first 3D implementation of the JFP model has been done by Chauchat and Médale (2014). They developed a Finite Element Method (FEM) model

to compute the steady-state of dense granular flow. They pointed out two key points to get a successful implementation: (I) the way to deal with the tricky pressure-dependent visco-plastic rheology within an incompressible flow solver; (II) the capability to solve efficiently such very stiff non-linear algebraic systems. They stressed the need of a regularization of the viscosity function both for the divergence as $\dot{\gamma} \rightarrow 0$ and for the pressure term therein, as it might become negative in some part of the domain. They tested three different regularization for the viscosity plus one more developed specifically for the $\mu(I)$ rheology, and found the latter one to perform better:

$$\eta = \mu(I) \frac{p}{\sqrt{\dot{\gamma}^2 + \lambda_\eta^2}}, \quad (2.11)$$

where λ_η is the regularization parameter. Regarding the pressure, they proposed the following equation:

$$p_{reg} = p + \sqrt{p^2 + \lambda_p^2}, \quad (2.12)$$

where λ_p is the regularization parameter and p_{reg} is the pressure to be used in the viscosity law. Despite the 3D implementation, they performed two quasi-2D simulations, in which the computational grids have only one cell along the depth.

Regarding the rotating drum problem, few attempts have been made to check the validity of a local-rheology approach. Renouf et al. (2005) showed in 2D DEM simulations that the friction law $\mu(I)$ is locally satisfied along the profile, while Orpe and Khakhar (2007) have shown in experiments

a reasonable agreement when the increase in friction coefficient with I is considered, even if the coefficient of friction is found to be significantly higher at high local flow rates (corresponding to high rotational speeds), which is not in agreement with the model. It must be said that, owing to the non-uniformity of the flow, a tensorial generalization should have been used to test the local rheology in this configuration.

The JFP model seems to describe dense granular flow very well, but Forterre and Pouliquen (2008) pointed out some limits of the approach, mainly concerning the yield criterion. The JFP model implement the flow threshold as a Drucker–Prager criterion, but the actual transition between flowing and jammed grains appears more complex and seems to involve shear bands (Jop, 2008) and hysteresis (Rajchenbach, 1990). Also the transition to the collisional rapid flow for $I > 0.3$ does not seem to be captured by the model. Eventually, jammed grains in 3D flow geometries (e.g. rotating cylinders or heaps) undergo a creep motion with an exponentially decaying velocity that (they claim) is not captured by the model. We will discuss the limits of the JFP constitutive equation in Chapter 4. Some non-local extension of the JFP model have been recently proposed to overcome some of these limits (Pouliquen and Forterre, 2009; Sun and Sundaresan, 2011; Kamrin and Koval, 2012; Bouzid et al., 2013; Henann and Kamrin, 2014).

To the best of our knowledge, there is not any fully 3D numerical work which tackles a complex flow using a continuum approach.

Materials and methods

3.1 Materials and geometries

The aim of this thesis is to investigate the flow behavior of granular materials in horizontal axial-rotating cylinders. We conducted our numerical experiments so as to investigate the effect of the three dimensionless parameters defined in equation (2.1). We also took into account the slippage at the cylinder walls via an additional parameter β , which is 0 in case of complete slip and 1 in case of adherence (see section 3.2 for its definition).

We systematically investigated the effect of the three dimensionless parameters $Fr = \Omega^2 R/g$, AR and D/d_p (see equation (2.1) for their definitions), for $\beta = 0.1$:

$$Fr = \begin{cases} 7.0 \cdot 10^{-5}, 2.8 \cdot 10^{-4}, 1.7 \cdot 10^{-3}, 7.0 \cdot 10^{-3}, \\ 1.6 \cdot 10^{-2}, 2.8 \cdot 10^{-2}, 6.3 \cdot 10^{-2}, 1.1 \cdot 10^{-1}; \end{cases}$$

$$AR = 0.05, 0.1, 0.2, 0.5, 1;$$

$$D/d_p = 1000, 2500.$$

Other simulations with different β values (namely $\beta = 0.2, 0.5, 1$) have been conducted at need.

According to (Jop et al., 2005), monodisperse granular materials can be fully characterized by the diameter d_p and the density ρ_p of a particle, and by the function $\mu(I)$ defined in equation 2.5, which accounts for the dissipative nature of a granular fluid, due to the inter-particle friction.

In this thesis we mainly used the parameter values by Jop et al. (2005), who were able to quantitatively model the flow of glass beads on a heap with the $\mu(I)$ -rheology:

$$\mu_s = \tan(20^\circ) \approx 0.364;$$

$$\mu_2 = \tan(33^\circ) \approx 0.649;$$

$$I_0 = 0.279;$$

plus the material properties:

$$d_p = 0.5mm;$$

$$\rho_p = 2450 \frac{kg}{m^3}.$$

Since the diameter of the cylinder appears in the definitions (eq. 2.1) of all the dimensionless parameters here studied, in order to vary each parameter independently from all the others, we fixed $D = 0.5m$ for all the simulations. Therefore we also performed simulations with $d_p = 0.2mm$ and, for the same reason, the cylinders considered here have five different widths, in order to investigate different aspect ratios. With $D = 0.5m$, the Froude numbers specified above corresponds to $\Omega = 0.5, 1, 2.5, 5, 7.5, 10, 15, 20 rpm$.

3.2 Governing equations

In this thesis, we solve the continuum dynamic equations by adopting the visco-plastic JFP constitutive model (Jop et al., 2006). The start point for the derivation of the final equations are the usual mass and momentum balance for a fluid:

$$\frac{\partial \rho}{\partial t} + \nabla \cdot (\rho \mathbf{u}) = 0, \quad (3.1)$$

$$\frac{\partial \rho \mathbf{u}}{\partial t} + \nabla \cdot (\rho \mathbf{u} \mathbf{u}) = -\nabla p + \nabla \cdot \boldsymbol{\tau} + \rho \mathbf{g} + \rho \mathbf{a}, \quad (3.2)$$

where \mathbf{g} is the gravitational force and $\rho \mathbf{a}$ is the sum of the other body forces acting in the system.

Since our aim is to investigate half-filled drums, our simulations must include two phases: a “liquid” phase L (the granular material) and a gaseous phase G , which we assumed having the physical properties of the air. In order to do so, a multiphase model need to be chosen.

Among the different models available to describe multiphase systems, we focused on the Volume of Fluid approach (hereinafter *VoF*, firstly proposed by Hirt and Nichols, 1981). VoF model treats the two phases as a single whole fluid (so with unique velocity and pressure fields) with physical properties varying through space and time. It introduces a phase volume fraction α which represent the fraction occupied by one of the phases (e.g. the liquid phase L) in each control volume, and varies from 0 (air only) to 1 (fluid only). The interface is postulated to be at $\alpha = 0.5$. Such a model has also been chosen by Lagrée et al. (2011) to perform their 2D simulations.

The underlying idea of the VoF model is that the mixture can be described as a *single fluid* whose physical properties depends on the position and can be calculated as volume-weighted averages between properties of the pure phases:

$$\rho = \alpha\rho_L + (1 - \alpha)\rho_G, \quad (3.3)$$

$$\eta = \alpha\eta_L + (1 - \alpha)\eta_G \quad (3.4)$$

The VoF method introduces then another independent variable, the volume fraction α , for which an evolutive equation is needed: the model prescribes that α is simply advected through the domain:

$$\frac{\partial\alpha}{\partial t} + \nabla \cdot (\alpha\mathbf{u}) = 0 \quad (3.5)$$

So far, the proposed equations are valid for any biphasic fluid system. In order to implement the JFP model, we need to define the liquid phase as a granular phase, for which the stress tensor is given by equations (2.7)–(2.9), and the other as a gaseous phase having the physical properties of air, $\eta_{air} = 1.48 \cdot 10^{-5} Pa \cdot s$ and $\rho_{air} = 1 kg/m^3$. At this point, we introduce an hypothesis: both phases are considered incompressible. For the granular phase this comes from the assumption of neglecting the small expansion of the granular phase due to the flow (Jop et al., 2006), for the air phase this means that the maximum velocity is well below the speed of the sound. Following Jop et al. (2005), we fix the volume fraction ϕ of the granular phase to 0.6, which is in between the random close packing factor $\phi \approx 0.63$

and the packing factor of loosest possible particles in contact (the simple cubic configuration, having $\phi \approx 0.52$).

It should be noticed that ϕ and α are both grains volume fraction, but they have completely different meanings: ϕ is the packing factor, that is the volume fraction occupied by the solid sphere in their 3D arrangement in the bulk; α is the volume fraction of the granular phase considered as a whole fluid (i.e. with its voids), so with a density $\rho_{grain} = \phi\rho_p$, and is used to calculate the physical properties through space and time in each control volume: physical properties vary in time and space because of their dependence on α .

It is possible to demonstrate that, even if the introduction of a the volume fraction α leads to a position–dependent density field, the mass balance for the two–phase fluid reduce to the usual expression for incompressible fluids: $\nabla \cdot \mathbf{u} = 0$. The ingredients to get this result are the convective equation (3.5) for the scalar α and the linearity of equation (3.3). In other words the following two sets of equations are equivalent for constant ρ_L and ρ_G :

$$\left\{ \begin{array}{l} \frac{\partial \rho}{\partial t} + \nabla \cdot (\rho \mathbf{u}) = 0 \\ \frac{\partial \alpha}{\partial t} + \nabla \cdot (\alpha \mathbf{u}) = 0 \\ \rho = \alpha \rho_L + (1 - \alpha) \rho_G \end{array} \right. \iff \left\{ \begin{array}{l} \nabla \cdot \mathbf{u} = 0 \\ \frac{\partial \alpha}{\partial t} + \nabla \cdot (\alpha \mathbf{u}) = 0 \\ \rho = \alpha \rho_L + (1 - \alpha) \rho_G \end{array} \right. \quad (3.6)$$

It must be noticed that only equation (3.3) must be rigorously linear, in order to choose the right–hand system in equation (3.6), and that different averaging function would be possible for the viscosity: e.g. Lagrée et al. (2011) implemented an harmonic average for the viscosity, instead of an

arithmetic one, by using $1/\eta = \alpha/\eta_L + (1 - \alpha)/\eta_G$.

The implementation of the JFP model is then straightforward: the density and the viscosity of the L -phase in equations (3.3) and (3.4) are replaced by the expressions for granular materials:

$$\rho = \alpha\rho_{grain} + (1 - \alpha)\rho_{air}, \quad (3.7)$$

$$\eta = \alpha\eta_{grain}(\dot{\gamma}, p) + (1 - \alpha)\eta_{air} = \eta(\dot{\gamma}, p), \quad (3.8)$$

where η_{grain} was given in Section 2.5:

$$\eta_{grain}(\dot{\gamma}, p) = \mu(I) \frac{p}{\dot{\gamma}} \quad (2.9)$$

At this stage only the term \mathbf{a} in equation (3.2) has to be specified. To this end, we decided to write equations (3.1) and (3.2) in a Cartesian coordinate system *fixed to the rotating cylinder*, with the z -axis oriented along the axis of the cylinder and the origin in its half-width, thus implying a rotating gravity $\mathbf{g}(t)$ and cylinder walls with a zero velocity. This choice gives rise to fictitious forces which have to be included in the \mathbf{a} term. Defining \mathbf{r} as the radial position inside the cylinder, a constant rotational motion of the cylinder about its axis gives:

$$\mathbf{a} = 2\boldsymbol{\omega} \times \dot{\mathbf{r}} + \boldsymbol{\omega} \times (\boldsymbol{\omega} \times \mathbf{r}) + \dot{\boldsymbol{\omega}} \times \mathbf{r}, \quad (3.9)$$

where $\boldsymbol{\omega} = (0, 0, \Omega)$ is the angular velocity vector and the dotted quantities are time derivatives of the corresponding variables. The first two terms in equation (3.9) are the Coriolis acceleration and the centrifugal accelera-

tion. Since our simulations reach a constant angular velocity almost instantaneously (in $10^{-3}s$), the term $\dot{\boldsymbol{\omega}} \times \mathbf{r}$ has been neglected.

In order to write down the final set of equations as they have been implemented in the software used for their integration, we will proceed to some further elaboration of the pressure and gravity terms in the momentum balance equation. First of all, we introduce here the *reduced pressure*:

$$p^* = p - \rho \mathbf{g} \cdot \mathbf{r}, \quad (3.10)$$

where the time dependence of the gravity is omitted for simplicity. In order to introduce it in equation (3.2) we have to express ∇p in terms of ∇p^* . After some straightforward math, the result is:

$$-\nabla p + \rho \mathbf{g} = -\nabla p^* - (\mathbf{g} \cdot \mathbf{r}) \nabla \rho. \quad (3.11)$$

We can then summarize the equations of motion of a biphasic granular system in a rotating reference frame as follows:

$$\nabla \cdot \mathbf{u} = 0 \quad (3.12)$$

$$\begin{aligned} \frac{\partial \rho \mathbf{u}}{\partial t} + \nabla \cdot (\rho \mathbf{u} \mathbf{u}) = & -\nabla p^* + \nabla \cdot \left[\eta(\dot{\gamma}, p) \left(\nabla \mathbf{u} + \nabla \mathbf{u}^T \right) \right] + \\ & - (\mathbf{g} \cdot \mathbf{r}) \nabla \rho + \rho [2\boldsymbol{\omega} \times \mathbf{u} + \boldsymbol{\omega} \times (\boldsymbol{\omega} \times \mathbf{r})] \end{aligned} \quad (3.13)$$

$$\frac{\partial \alpha}{\partial t} + \nabla \cdot (\alpha \mathbf{u}) = 0 \quad (3.14)$$

with p^* given by equation (3.10), the density and the viscosity by equa-

tions (3.7) and (3.8), and with the following auxiliary equations:

$$\eta_{grain}(\dot{\gamma}, p) = \left(\mu_s + \frac{\mu_2 - \mu_s}{I_0/I + 1} \right) \frac{p}{\dot{\gamma}} \quad (3.15)$$

$$I = \frac{d_p \dot{\gamma}}{\sqrt{p/\rho_p}} \quad (3.16)$$

Our flow configuration has a planar symmetry that can be used to reduce the dimension of the computational domain. Only one half of the cylinder has been simulated and a symmetry condition has been enforced on the central symmetry plane $z = 0$:

$$\begin{cases} \mathbf{u} \cdot \hat{\mathbf{z}} = 0 \\ \nabla \mathbf{u} \cdot \hat{\mathbf{z}} = \mathbf{0} \end{cases} \quad (3.17)$$

and

$$\nabla \alpha \cdot \hat{\mathbf{z}} = 0 \quad (3.18)$$

where $\hat{\mathbf{z}}$ is the normal to the center plane.

We used a partial slip boundary condition on the walls; in a reference system fixed to the rotating cylinder the velocity of the wall is zero and the BC at walls reads:

$$\begin{cases} \mathbf{u} \cdot \mathbf{n}_w = 0 \\ \beta \mathbf{u} + (1 - \beta) \nabla \mathbf{u} \cdot \mathbf{n}_w = \mathbf{0} \end{cases} \quad (3.19)$$

where \mathbf{n}_w is the normal to the boundary.

The parameter β tunes the degree of slipping at the wall: $\beta = 1$ means complete adherence ($\mathbf{u} = \mathbf{0}$), $\beta = 0$ means complete slip ($\nabla \mathbf{u} \cdot \mathbf{n}_w = \mathbf{0}$).

The boundary condition for α at walls is a zero-gradient condition:

$$\nabla\alpha \cdot \mathbf{n}_w = 0. \quad (3.20)$$

Few more words are worth about the absolute pressure p contained in the viscosity function. p is supposed to be the *compressive* stress that grains “feel” in their dense state. Jop et al. (2006) imposed $p = 0$ on the free-surface boundary of their computational domain, as if the first layer of grains might be considered “free”, actually implying a zero viscosity on top of the flowing layer. In this thesis we adhere to the idea of compressive pressure, and put to zero any negative pressure contribution inside the viscosity equation. In other word, we put the viscosity to zero whenever the local pressure is negative. Pressure is scaled with respect to the center of the cylinder, where its value is 0.

Finally, since the viscosity diverges as $\dot{\gamma} \rightarrow 0$, a further regularization is needed: the approach chosen is to bound the viscosity function to a maximum value $\eta_{max} = \rho_{grain} 100 \frac{m^2}{s}$, which is $\sim 10^8$ times the viscosity of water. The accuracy of this approach is discussed in section 4.8. The need for these normalizations is confirmed by Chauchat and Médale (2014), but our approach is slightly different from their choices.

3.3 Numerical method

To integrate the above equation along with their boundary conditions, we used the open source CFD software package OpenFOAM (Weller et al., 1998).

OpenFOAM is structured as a library of routines, so it is highly modular, and the source code is fully accessible and editable, so it is also very versatile.

We modified the *interFoam* solver, which solves the equations of motion for a two-phases incompressible fluid with a specific version of the VoF model (Berberović et al., 2009). In this formulation, the VoF model employs an additional term in equation (3.14), which is non-zero only close to the interface, and acts as a “compression term” to keep the interface sharp.

We implemented the JFP model in a standalone routine and we modified the source code of *interFoam* in order to implement the rotating reference frame. This basically involved the implementation of a time-dependent gravity and the addition of a source term in the momentum equation (the fictitious forces \mathbf{a}).

interFoam implements the PIMPLE algorithm, which is an algorithm for solving transient problem. PIMPLE is a blending of the PISO (Pressure-Implicit with Splitting of Operators, Issa et al., 1986) and the SIMPLE (Semi-Implicit Method for Pressure Linked Equations, Patankar, 1980) algorithms: it essentially includes one or more PISO loops inside one or more outer SIMPLE loops, all of them made at each time step. These methods belong to the broad category of the pressure-correction methods: they are based on the derivation of a *pressure equation* from the continuity and momentum equations, which enforces mass conservation (Ferziger and Perić, 2001).

The inner PISO loop basically guess a velocity field from a linearized version of the momentum equation using the velocity (for the non-linear and the fictitious terms and for the), pressure and density fields from the last available solution (i.e. the previous time step or the previous *outer loop*); then it uses

the pressure equation to calculate a correction for the velocity field. This last step can be repeated until corrections are negligible. The outer SIMPLE loop allows to update the velocity field (i.e. to recalculate the velocity field with updated density field and updated non-linear fictitious and pressure terms) before the next inner PISO loop. The number of SIMPLE iterations coincides with the number of PISO loops and to the freshly calculated velocity field, while the number of PISO iterations coincides with the number of pressure corrections applied to the same velocity field. The PIMPLE algorithm has been devised to take advantage of the SIMPLE under-relaxation, and allows for larger time steps than the pure PISO algorithm. In our simulation we performed 3 inner cycles and a number of outer cycles as to have the residual of the solution below 10^{-8} for both pressure and velocity. These algorithm can be applied regardless the actual solver for the algebraic systems generated by the discretization. In our simulations we used the solvers reported in table 3.1. Moreover, the code allow to solve equation (3.14) with sub-steps within each time-step, in order to better describe the material flux. We choose to solve the volume fraction field three times per time-step.

The presence of a pressure equation determines the need of boundary conditions for the pressure itself. This is, in our opinion, one of the major drawbacks in using pressure-correction methods. We imposed a pressure gradient at the walls equal to the hydrostatic one:

$$\nabla p = \rho(\mathbf{g} \cdot \mathbf{n}_w), \quad (3.21)$$

	SOLVER	PRECONDITIONER
p^*	GAMG (Generalised geometric–algebraic multi–grid)	
p_{corr}	PCG (Preconditioned conjugate gradient)	DIC (Diagonal incomplete–Cholesky)
\mathbf{u}	PBiCG (Preconditioned bi–conjugate gradient)	DILU (Diagonal incomplete–LU)
α	MULES (Multidimensional universal limiter for explicit solution)	

Table 3.1: Solvers for each variable. p_{corr} is an additional variable which stores the corrections to the flux calculated with the pressure equation.

which, in terms of p^* , reads:

$$\nabla p^* = -\nabla \rho (\mathbf{g} \cdot \mathbf{r}). \quad (3.22)$$

Of course, on the symmetry plane it is:

$$\nabla p^* \cdot \hat{\mathbf{z}} = 0. \quad (3.23)$$

A thorough description of *interFoam*, together with few validation cases, can be found in Deshpande et al. (2012).

3.4 Convergence tests

The discretization of the spatial domain is a key point for the overall performance of the code. In order to minimize the number of computational cells and to improve the interpolation order at the cell face (required by a FVM

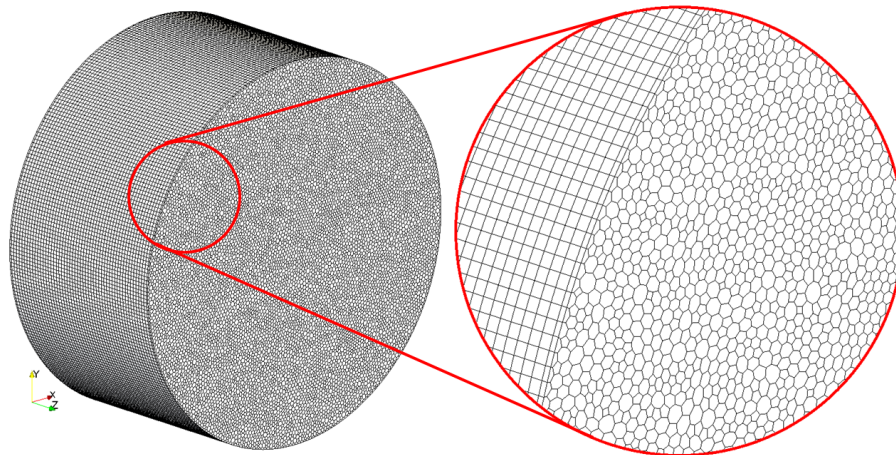


Figure 3.1: Sketch of the polygonal mesh for $AR = 1$ with a close-up of the lateral wall and the symmetry plane.

code to calculate the flux between two adjacent cells) we generated *polygonal* meshes. A sketch of such mesh can be seen in Figure 3.1.

All the simulations presented in this thesis have been conducted over the time-span needed to complete one single cycle. As Figures 3.2 show, the systems do not attain a steady state, but they rather display a steady regime, where small oscillations are still present. Because of that, during the preliminary convergence tests, we often found the evaluation of the error at a specified time quite inaccurate, while the trends of both local and integral quantities was the same in average. So, in order to smooth out the oscillations, we averaged all the quantities over the last half of the cycle, where all the simulations were in the steady regime. The error between the chosen mesh and the finer one ($\sim 4\times$ cells) was always below the 5%.

Regarding the time step, it is adapted throughout the calculation in order to match a local stability criteria based on the Courant number Co (Berberović et al., 2009), which prescribes that a cell can not abide a volu-

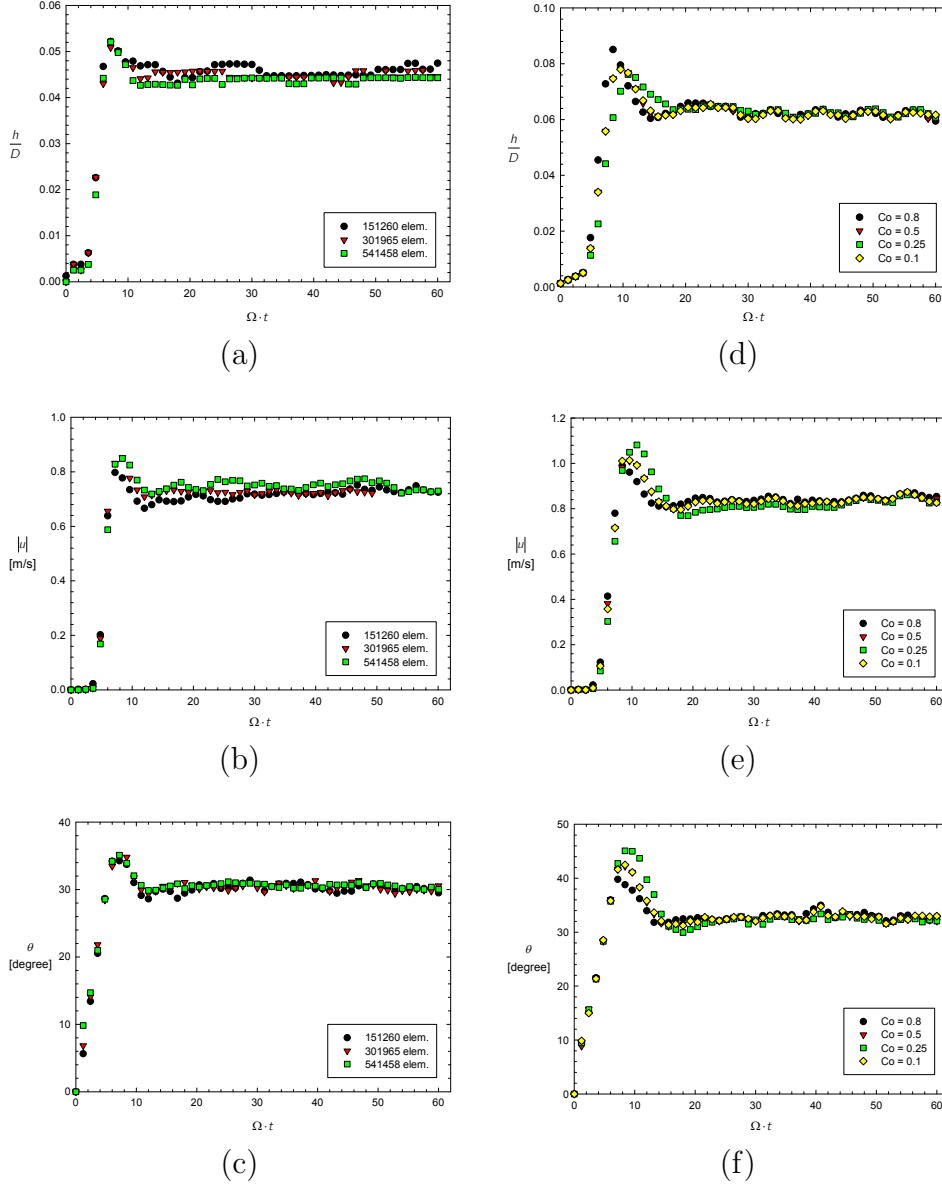


Figure 3.2: Temporal evolutions of the flow thickness (a,e), the velocity at the midpoint of the free surface (b,d) and the inclination of the free surface (c,f) at the center plane parametric in the number of element of the computational grid (a-c) and the Courant number (d-f). Spatial convergence presented for $D/d_p = 1000$, $AR = 0.2$, $\Omega = 5rpm$, temporal convergence for $D/d_p = 2500$, $AR = 0.1$, $\Omega = 10rpm$, both having $\beta = 0.1$.

metric flow bigger than a certain fraction of its volume over the time step. The local Courant number, calculated with values from the last time step, is compared with a limit value: if anywhere in the mesh the local Co exceeds the limit value, the time step is decreased in order to have a new local Co below the threshold. In other words, the higher the Courant number limit, the higher the time step allowed. In the legends of Figures 3.2 (d-f) is indeed reported the Courant limit. A maximum time step size of $10^{-3}s$ has also been used for all the simulations.

Figures 3.2 reports the converge trials for two of our simulations, but the convergence has been evaluated at each major changes in the parameters (e.g., much finer grids in axial direction have been used for the no-slip cases). The figure shows that, even if not perfectly superimposed, the simulations with more cells or with shorter time steps show essentially the same behavior as those with less cells and larger time steps, thus there are no more effects linked to the degree of refinement of the spatial and temporal domain.

4.1 Introduction

We investigated the dense granular flow of monodisperse spheres inside a cylinder rotating about its axis at different values of angular velocity Ω , diameter ratio D/d_p , aspect ratio AR and slip parameter β . Hereinafter only results for $D/d_p = 1000$ will be shown, since cases with $D/d_p = 2500$ are within the error bars of the formers. If not stated otherwise, the following results are to be considered as having slip parameter $\beta = 0.1$. Moreover, we will only show quantities in the fixed reference frame and we will use the same symbols used in Chapter 3 for the cylinder-fixed reference frame.

Figures 4.1 show some of the probing lines used in the following graphs. First of all, we will analyze data taken both at the center plane of the cylinder, where we impose the symmetry condition, and near the end wall. Data obtained probing the system along the red lines are referred to as *radial*, since they are perpendicular to the free surface and intersect the axis of the cylinder. Since the free surface does not generally pass through the axis of

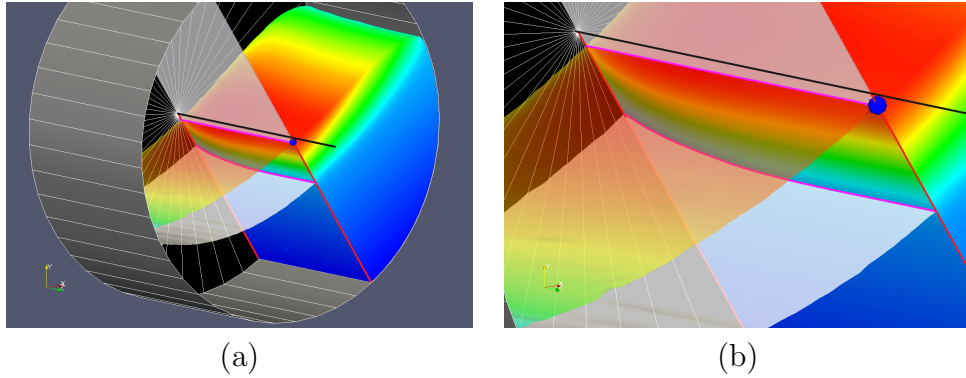


Figure 4.1: Full view (a) and a close-up (b) of a cut of the granular phase with the indication of the sampling lines. The semi-transparent surfaces are the free surface and the boundary between the flowing layer and the fixed bed.

the cylinder, the coordinate system will be $r - r_{top}$, where r_{top} is the intercept of the line with the free surface; in the case of data taken at the center, r_{top} is the blue sphere in Figures 4.1. In other words, the radial coordinate will be systematically (i.e. individually during the post-process of each simulation) shifted so as to have its origin on the free-surface of the granular phase.

Another kind of profile will be called “axial” and is the profile along the curves identified by the intersection of a plane generated by the axis of the cylinder and the perpendicular to the free surface (the semi-transparent plane in Figure 4.1) and the free surface itself or the bottom of the flowing layer (both in magenta in Figure 4.1). Actually, the curves are the projection of the axis on the free surface or on the bottom of the flowing layer. The abscissa in this case is the z -component of the points on the curve, divided by the half-depth $W/2$ of the cylinder: $\frac{z}{W/2}$ is 0 at the center of the cylinder and -1 at the wall.

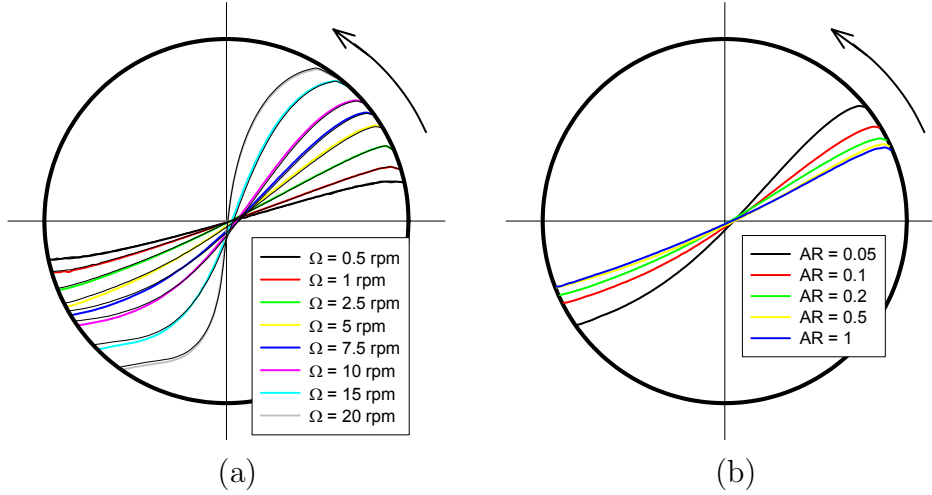


Figure 4.2: The free surfaces at the center of a cylinder with $D/d_p = 1000$, $AR = 0.1$ and $\beta = 0.1$ (a) and with $D/d_p = 1000$, $\Omega = 5 \text{ rpm}$ and $\beta = 0.1$ (b). Thin black lines in (a) are the correspondent free surfaces at $D/d_p = 2500$.

4.2 Free-surface

The rolling flow regime is characterized by a flat surface of the granular media, while the cascading regime shows a S -shaped free surface. There is not any clear separation between the two regimes, and the transition is gradual and smooth.

Figure 4.2 (a) shows the free surfaces for $D/d_p = 1000$, $AR = 0.1$ and $\beta = 0.1$. All the surfaces are S -shaped, but the curvature is almost zero for low angular velocities, and increases with increasing Ω . Consistently with the literature (see e.g. Rajchenbach, 1990), as the angular velocity is increased, the inertia of the grains which enter the flowing layer deforms the free surface. Figure 4.2 (b) shows that as the aspect ratio is decreased, the free surface is brought higher by the closer walls. The slip parameter β has only a very

weak effect on the shape of the free surface and thus is not reported.

Looking at the extreme parts of the high velocities free surfaces in Figure 4.2 (a), i.e. looking at the free surface(s) near the cylinder wall, it is possible to see that they are almost tangent to the lateral wall of the cylinder in the upper part, and that they are almost perpendicular to it in the lower part. In real experiments (see e.g. Rajchenbach, 1990) the grains comes out of the bed with a tangential velocity (due to rotation) which makes it continue to follow the rigid path for a little while and, at the bottom of the free surface, it hits the lateral wall before being dragged downward. Our numerical profiles somehow reflect these behaviors, although, of course, detachment of individual grains from the free surface and entering the cataracting regime cannot appear in our simulation results, which are obtained under the assumption of constant ϕ .

4.3 Flowing layer thickness

The thickness of the flowing layer h has been measured as reported in Félix et al. (2007), i.e. by measuring the distance from the free surface of the zero-velocity point along the cylinder radius perpendicular to the interface. Looking at Figures 4.1, h is the distance between the two magenta lines.

Figure 4.3 shows the trends of the flow depth with the angular velocity of the cylinder both at the center plane and near the wall. The thickness of the flowing layer measured in the center plane of the cylinder steadily increases with increasing angular velocity throughout the explored range. The behavior at the end wall is different: the flowing layer is not substantially

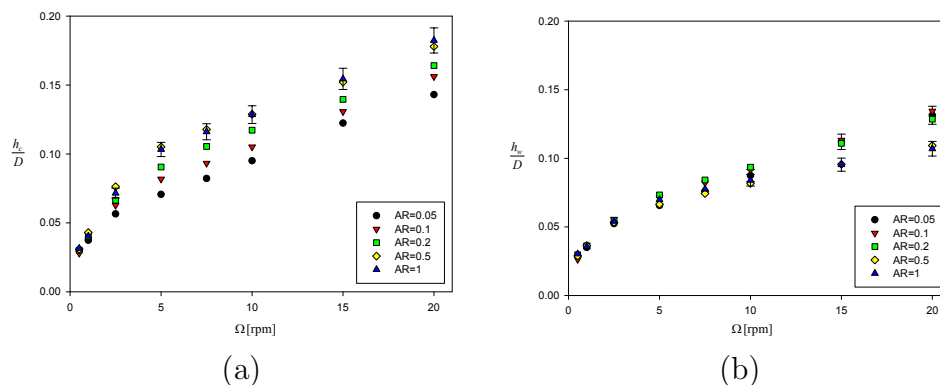


Figure 4.3: Thickness of the flowing layer versus Ω at the center plane (a) and near the wall (b) for $D/d_p = 1000$ and $\beta = 0.1$. Error bars are reported only for the most severe cases.

affected by the aspect ratio of the cylinder, and minor differences between long ($AR = 0.5, 1$) and short cylinders ($AR = 0.05, 0.1, 0.2$) can be seen only at very high rotation rates. This is consistent with the observation of Félix et al. (2007) that the width of the cylinder does not affect the flow thickness near the wall.

Figure 4.4 shows the ratio between the flow depths at the center and near the wall for various diameters (open and full symbols) and aspect ratios. As already said, the results for both values of D/d_p are the same.

This plot demonstrates that the flowing layer can be significantly different at the center and near the wall and that the difference depends on the rotation rate of the cylinder and on its aspect ratio. For narrow cylinders, the depth ratio decrease with Ω and reaches a plateau quite soon. This means that the flowing layer depth increases both at the center and near the end wall with the same rate. This is not the case for cylinders having $AR = 1$: in this case a clear plateau is not present and the thickness ratio keeps decreasing

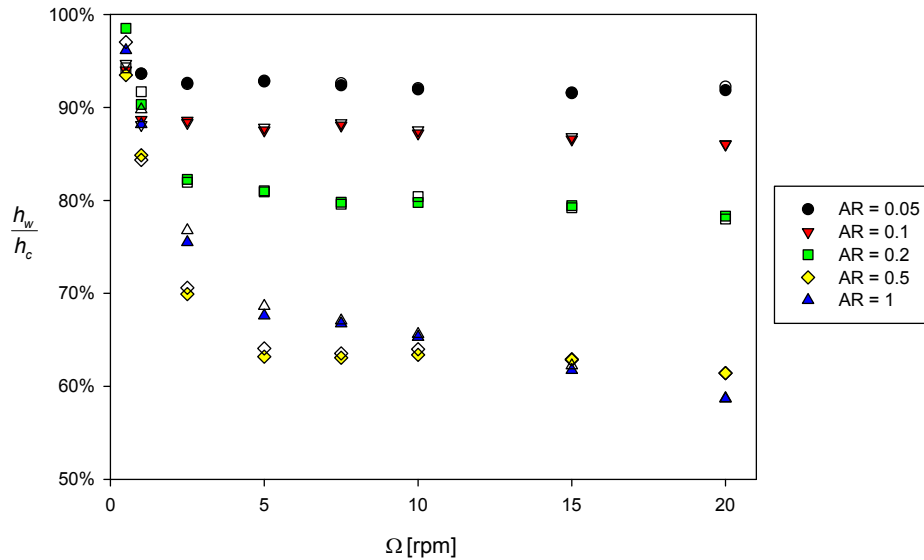


Figure 4.4: Ratio between the thicknesses of the flowing layer near the wall and at the center versus the aspect ratio for $\beta = 0.1$. Full symbols are for $D/d_p = 1000$, open ones are for $D/d_p = 2500$.

with angular velocity, i.e. the thickness of the flowing layer at the center plane increases faster than that near the wall. The different behavior might be linked to the separation of the two boundary layers, as conjectured by Pohlman et al. (2006a).

The fact that there are differences between the flowing layer thickness at the center or near the wall, even in the case of noticeable slip, is also shown in Figure 4.5. It displays a section of the flowing layers for the wider cylinder at various angular velocities and the same data rescaled by the depth at the center. Those curves are obtained by cutting the geometry with a plane passing through the axis of the cylinder and perpendicular to the free surface (see Figure 4.1).

The portions of the graphs above and below the curves represent respec-

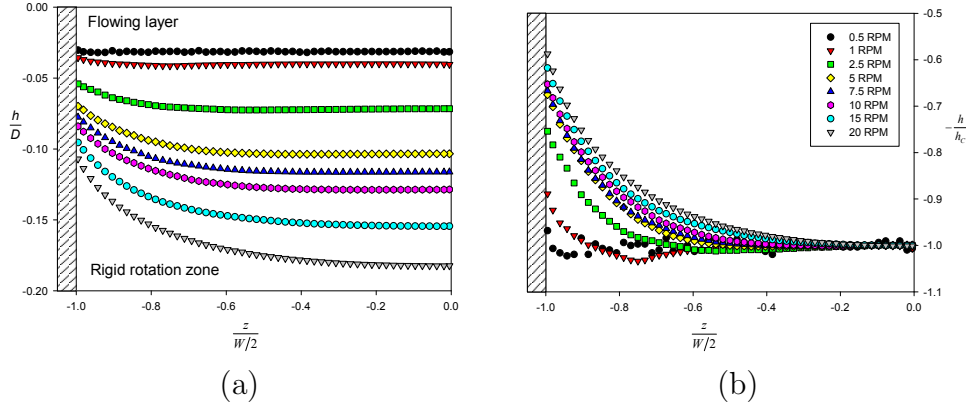


Figure 4.5: Axial profiles of the thickness of the flowing layer parametric in Ω (a) and a rescaled version of the same data (b) for $D/d_p = 1000$, $AR = 1$ and $\beta = 0.1$.

tively the flowing layer (the free surface is at $h/D = 0$) and the rigidly rotating zone. Going from low to high angular velocities, both the flow depth and wall effects increases. At high velocities, the rescaled curves tend to superimpose, which is another representation of the flattening behaviors in Figure 4.4.

4.3.1 AR and slip effects

Figure 4.6 shows the effect of the aspect ratio of the cylinder on the thickness of the flowing layer. There is a qualitative difference between the behaviors at the center plane and near the end wall. The flow layer thickness at the center of the cylinder increases with the aspect ratio, until it seems to reach a steady value. Near the wall, conversely, the flow depth displays a non-monotonic behavior, with a maximum at low angular rates. For high aspect ratios the flow depth at the wall seems to reach a plateau as well. Actually,

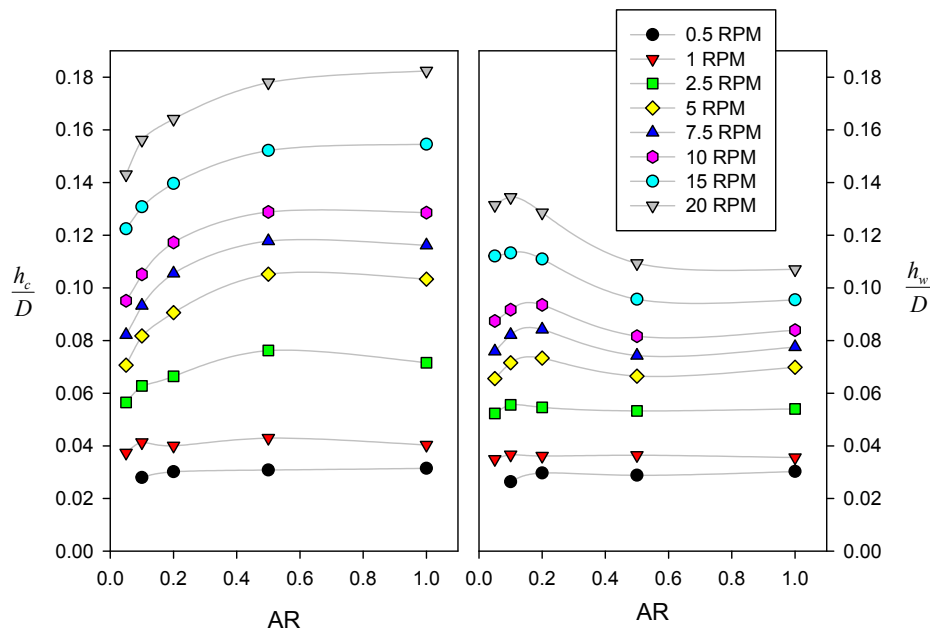


Figure 4.6: Effect of the aspect ratio AR on the flow depth at the center (left) and near the wall (right) of a rotating cylinder having $D/d_p = 1000$, $\Omega = 5rpm$ and $\beta = 0.1$

the non-linear behavior is weak: this might perhaps explain the common observation of a flowing layer independent on the width of the cylinder (see e.g. Félix et al., 2007).

Such observation is also supported by data on wall slip effect. Even if the slip regards the interactions between the particles and the wall, it does not affect thickness at the wall, and the only effect is on the thickness at the center. Figure 4.7 (a) shows the thickness of the flowing layer for $\Omega = 5rpm$ for various aspect ratios and for two slip conditions: the maximum slip investigated (on the left), and the complete adherence (on the right). The flow depth at the wall is the same for all the aspect ratios, and depends only on the slip. Figure 4.7 (b) shows how the curves vary with the wall slip: the

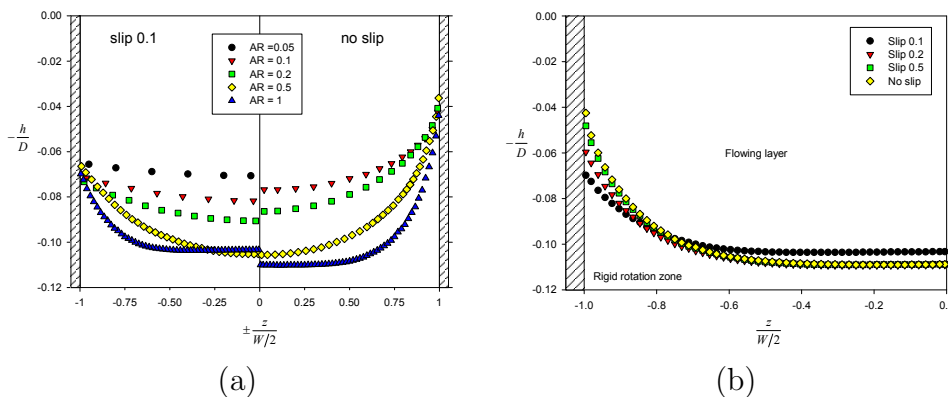


Figure 4.7: Axial profiles of the thickness of the flowing layer parametric in Ω (a) and a rescaled version of the same data (b) for $D/d_p = 1000$, $AR = 1$ and $\beta = 0.1$.

higher the adherence, the lower the flow depth at the wall.

It can be concluded that the flow depth at the wall is independent on the aspect ratio and depends only on the slippage of the boundary. Nevertheless, the flow depth at the center of a cylinder is usually significantly different from what can be seen through a transparent end-wall. The discrepancy rapidly increases as the aspect ratio and the angular velocity are increased.

4.4 Dynamic angle

Figure 4.8 shows the trends of the dynamic angle with the angular velocity of the rotating cylinder. The angles for the case with $D/d_p = 2500$ are the same as those shown in figure, as well as those near the wall. The only observed difference of few degrees ($\sim 2^\circ \div 4^\circ$) are between the center and the wall of the longest cylinders ($AR = 0.5, 1$, see Figure 4.9), which is consistent with the MRI experiments of Yamane et al. (1998) and Dury et al. (1998).

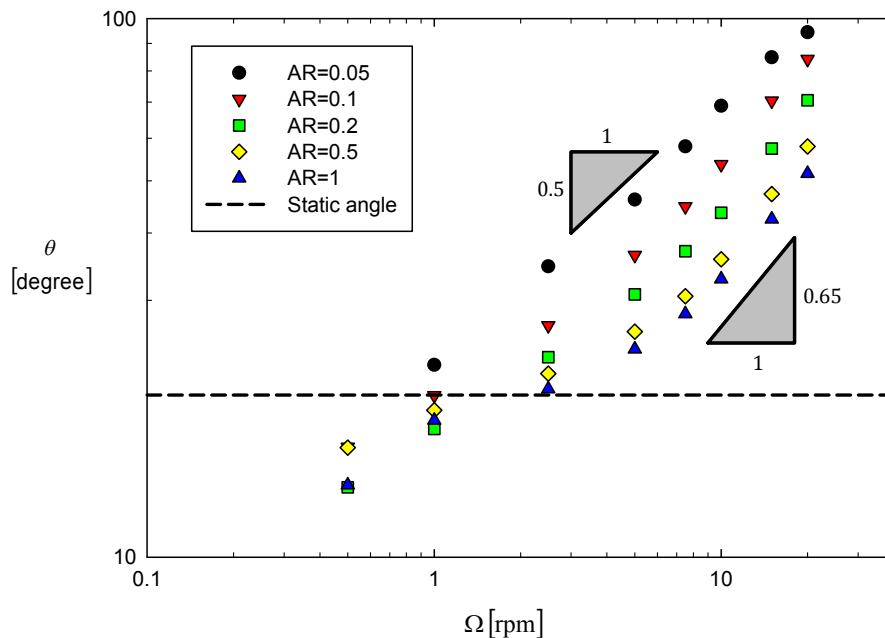


Figure 4.8: Dynamic angle versus Ω in cylinders having $D/d_p = 1000$ and $\beta = 0.1$

At high Ω the angle scales as $\theta \propto \Omega^{0.65}$ (except for $AR = 0.05$, for which a lower index is found). A less than linear power-law scaling is reported by Pöschel and Buchholtz (1995), who found an index equal to 0.8. At lower Ω the angles become lower than the static angle ($\arctan(\mu_s)$) and the curves tend to collapse towards a single trend. It must be noticed that the last point for $AR = 0.05$ is above 90° , which corresponds to a free surface tilted beyond the vertical. Angles higher than usual have already been reported in literature (Taberlet et al., 2003), but whether this is a physical behavior is questionable. The reason for both those unusual behaviors might be linked to our choice to fix the volume fraction $\phi = 0.6$, which might prevent the transitions to the slumping regime for low Ω and to the cataracting regime for high Ω . Further investigation are needed to clarify whether these behavior

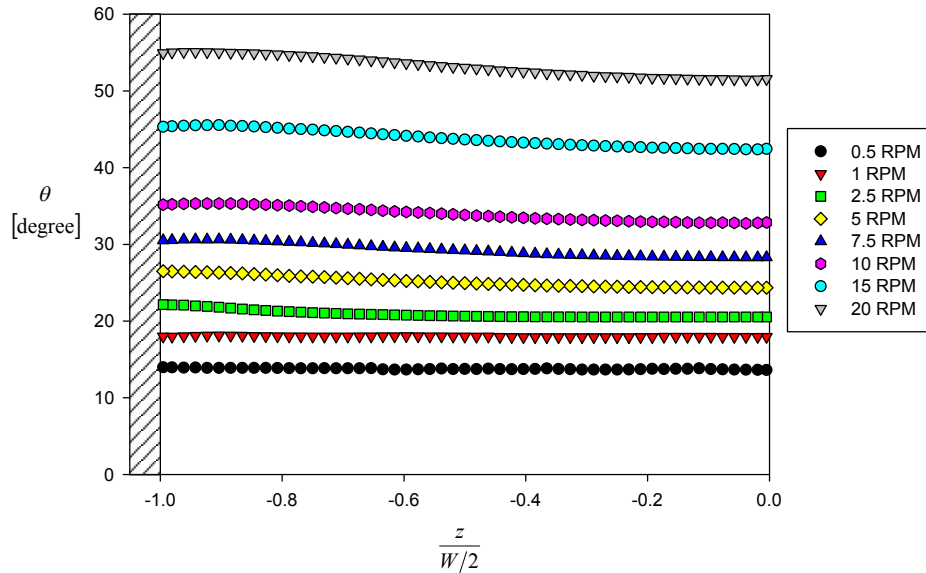


Figure 4.9: Axial profile of the dynamic angle parametric in Ω in cylinders having $D/d_p = 1000$, $AR = 1$ and $\beta = 0.1$

are physically realistic or not.

Figure 4.9 shows the profiles of dynamic angles along the center-line of the free surface in a cylinder with $AR = 1$ for various angular velocity. The angle is practically constant, but a difference between the center and the wall appears as the velocity is increased. Again, simulations with $\Omega = 0.5$, $1rpm$ show a lower dynamic angle than the static angle of repose.

This difference is also affected by the aspect ratio, as demonstrated in Figure 4.10, which shows the dynamic angle of the free surface along the axis for the same angular velocity but at various aspect ratios.

Curves for different wall slip values are superimposed to those shown in Figures 4.9 and 4.10: it is apparent that the wall slip does not influence the dynamic angle, which then appear to depends only on the angular velocity and the aspect ratio.

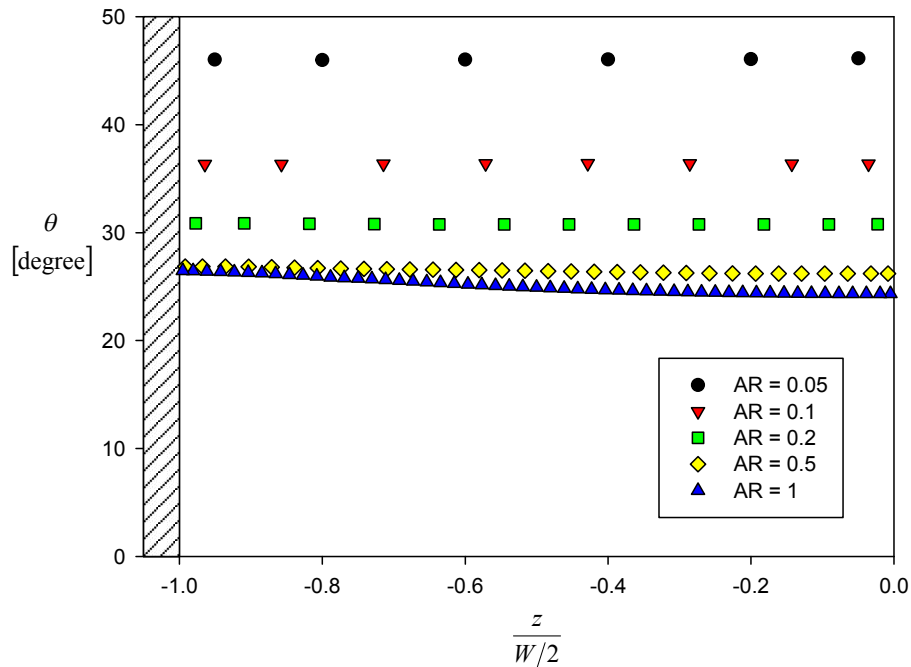


Figure 4.10: Axial profile of the dynamic angle parametric in AR in cylinders having $D/d_p = 1000$, $\Omega = 5rpm$ and $\beta = 0.1$

4.5 Velocity profiles

The profiles in the following two sections will be presented at different values of the three parameters Ω , AR and β . Those parameters will be varied starting from a common origin in the parameter space, which is $\Omega = 5rpm$, $AR = 0.1$ and $\beta = 0.1$. For example, a graph parametric in AR will be at $\Omega = 5rpm$ and $\beta = 0.1$, while a graph parametric in β will have $\Omega = 5rpm$ and $AR = 0.1$.

Figure 4.11 shows the typical radial profile obtained at the center and near the wall of the cylinder (the abscissa of the near-wall graph has been reversed to facilitate the comparison). It is trivial to observe an increase of the velocity as the cylinder angular velocity is increased or comparing the

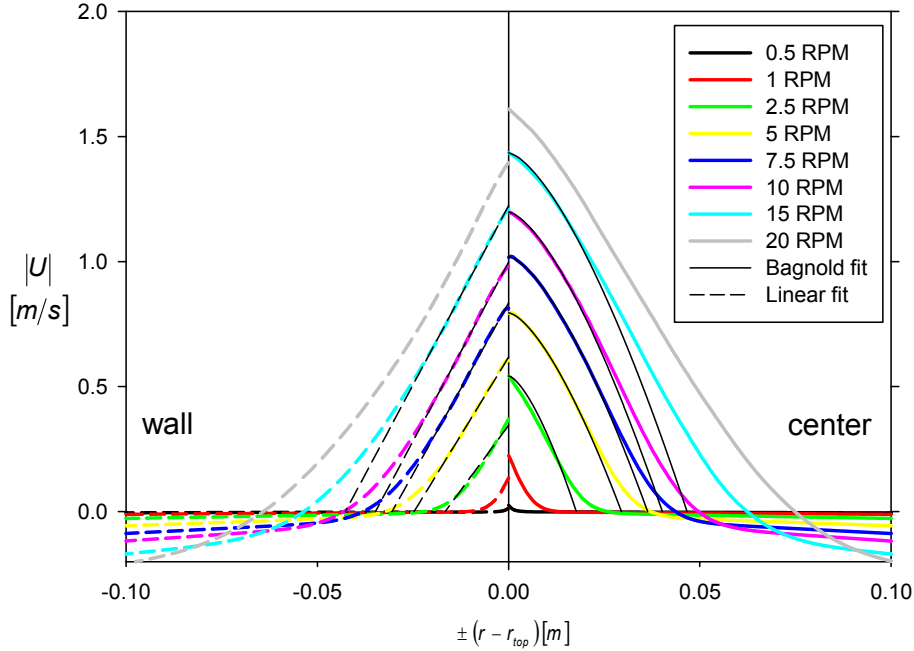


Figure 4.11: Radial velocity profiles at center and near the wall parametric in Ω . Solid lines on the right refers to the center and dashed lines on the left refer to the end wall. Thin black lines are fit of the numerical data.

center and the wall. The important effect of the wall is on the shape of the velocity profiles, even for a cylinder with $AR = 0.1$. While the profiles near the wall are linear (dashed black lines in figure), the profiles at the center have an increasing curvature. Solid black lines in figures represent the Bagnold scaling (Bagnold, 1954):

$$U = U_{top} \left[1 - a (r - r_{top})^{\frac{3}{2}} \right] \quad (4.1)$$

where U_{top} is the velocity in r_{top} and a is a fitting parameter. Bagnold scaling is nicely observed to hold for intermediate angular velocities, at the cylinder

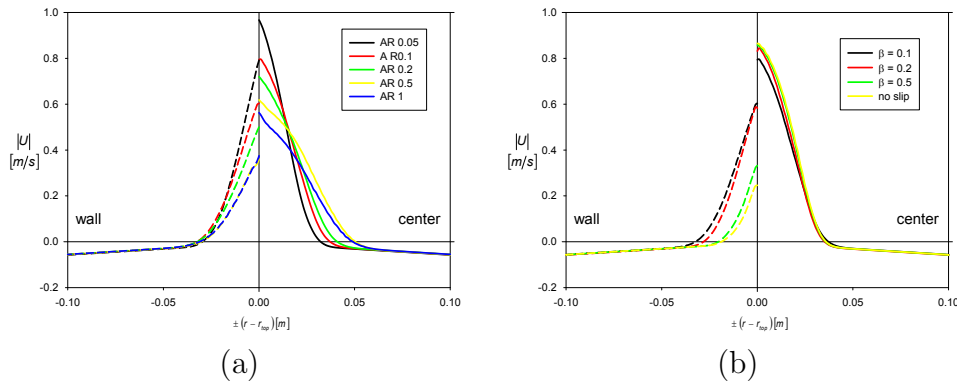


Figure 4.12: Radial velocity profiles at center and near the wall parametric in AR and β .

center.

Since typical experimental cylinders are inspected through a transparent end wall, a linear velocity profile is a very common observation in almost all the scientific literature, and it raised many questions on the qualitative difference between heap flows and inclined plane flows (GDR MiDi, 2004). A non-linear velocity profile has been observed in the center of a very long rotating drum ($AR > 50$) by Parker et al. (1997) and shown in Figures 2.6.

The effect of AR is shown in Figure 4.12 (a): consistently with the literature, the velocity on the free surface increases as the aspect ratio decreases. As expected and shown in Figure 4.12 (b), the slip influences the velocity profile only near the wall: while the center is almost unaffected by the imposed boundary condition, the velocity near the wall increases with increasing slip.

Figure 4.13 shows the axial profiles of the velocity. The profiles show a maximum (as those in Figure 4.19) which is $\sim 5\%$ higher than the velocity at the center.

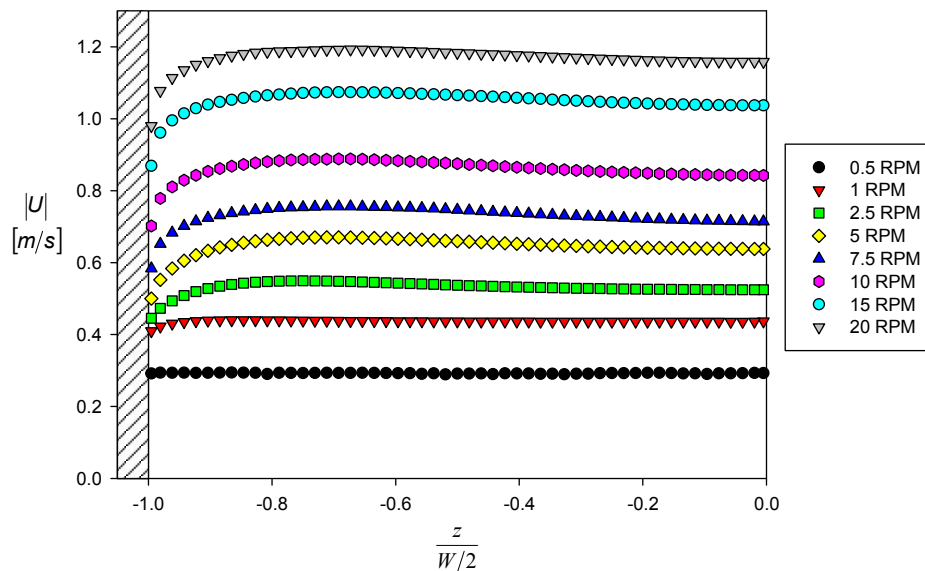


Figure 4.13: Axial profiles of the velocity parametric in Ω .

4.6 Inertial number profiles

Figure 4.14 shows the computed radial profiles of the inertial number I . For all our simulations, its value is below 0.1 everywhere in the domain except at the surface of the grains close to the wall. The profiles at the center start with an almost constant value and then start to decay exponentially; at a certain point there is a sudden change in the rate of decaying (the slope of linear parts in log–lin graph) when the viscosity normalization is applied. Beyond that point the motion is rigid and the inertial number has dropped well below the dense flow limit. This will be further discussed in Section 4.8.

The profiles for $\Omega = 0.5rpm$ are qualitatively different from the others, maybe because the system is approaching the transition to the slumping regime. However, our code failed to simulate the intermittent behavior typical of this regime.

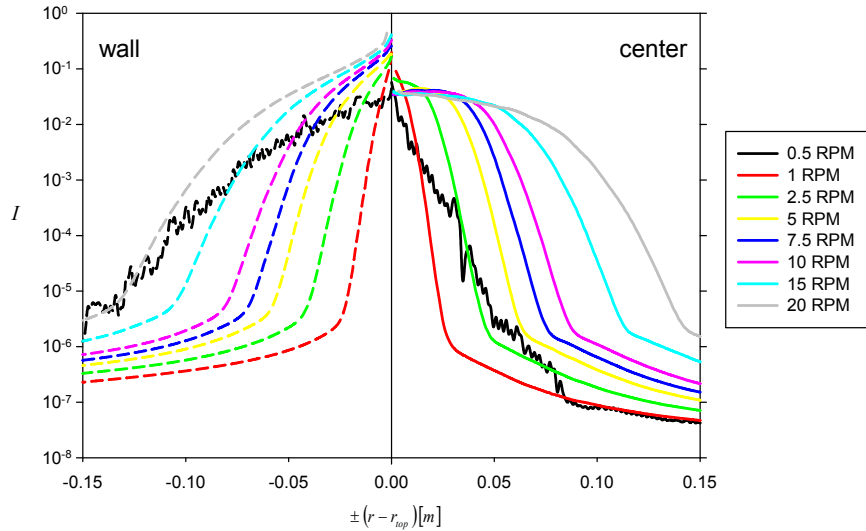


Figure 4.14: Radial profiles of the inertial number at center and near the wall parametric in Ω . Solid lines on the right refers to the center and dashed lines on the left refer to the end wall.

The wall slip and the aspect ratio do not influence the inertial number profile to a significant extent.

4.7 Surface velocity

Figures in this section will show contours of the axial component of the free-surface velocity. Since free surfaces are S -shaped, graphs are projections of the free surface on a plane parallel to the axis of the cylinder, passing through the extremes of the S shape. The vertical axis coincides with the axis of the cylinder. This is the numerical equivalent of what Pohlman et al. (2006a) did experimentally.

Figure 4.15 shows the contour of the axial component of the surface velocity at various angular velocity of the drum for the case $D/d_p = 1000$, $AR = 1$

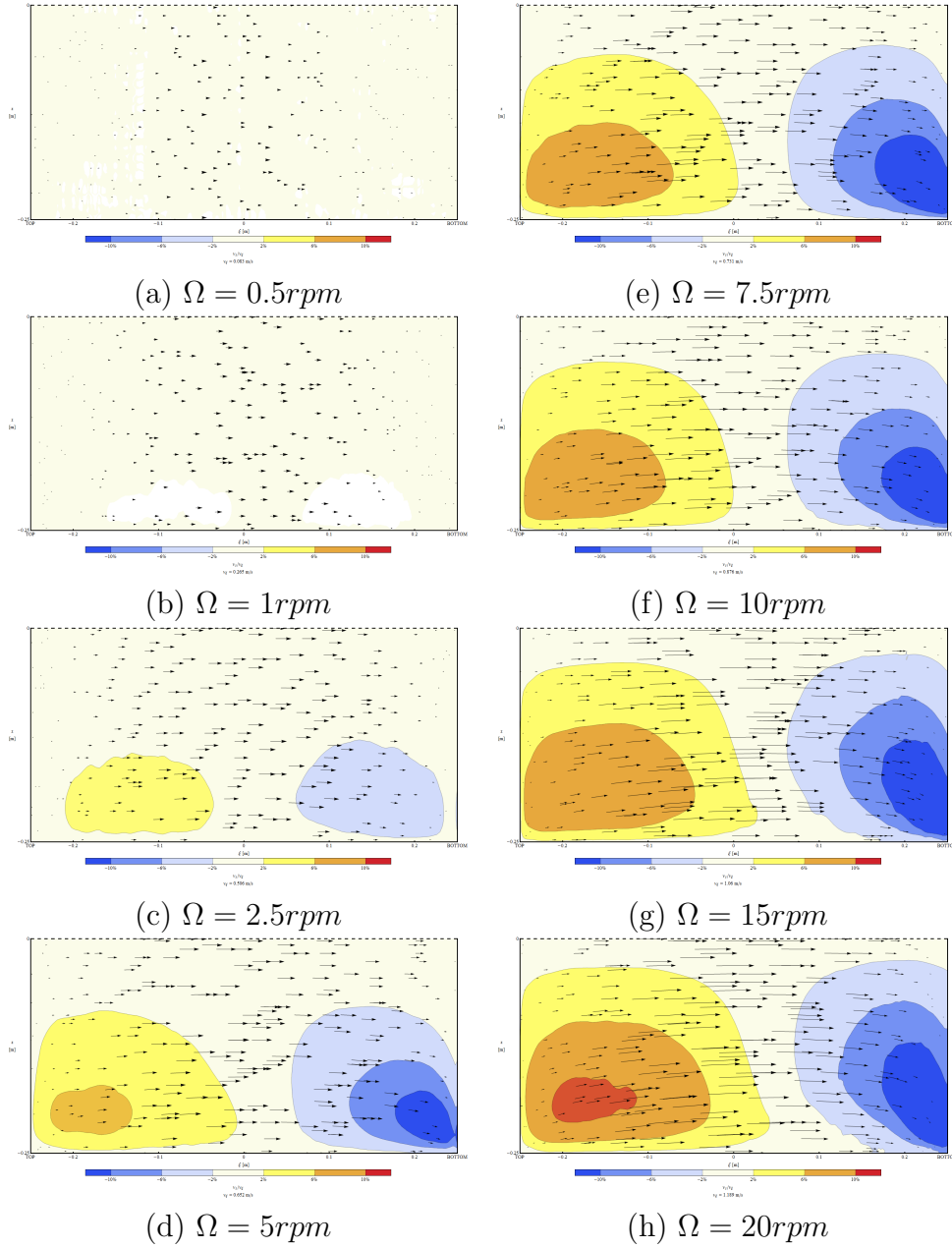


Figure 4.15: Contours of the free-surface velocity parametric in Ω . Velocities are divided by the one at the center of the free surface on the center plane ($\xi = z = 0$). The top of the free surface is on the left and the center plane on top.

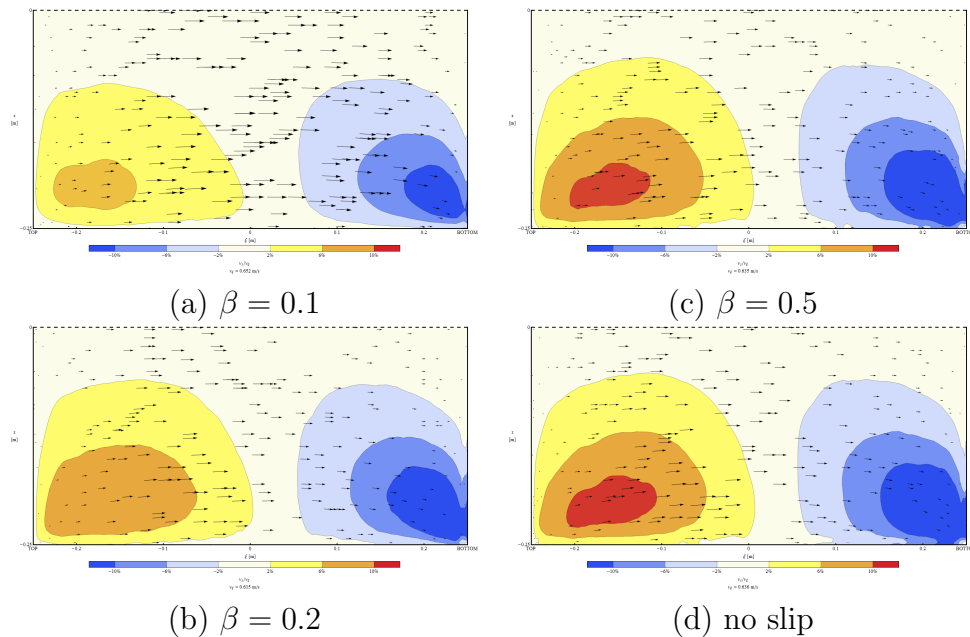


Figure 4.16: Contours of the free-surface velocity parametric in β .

and $\beta = 0.1$. The coordinate ξ , which goes from the top to the bottom of the free surface itself, is the projection of a point of the free surface on the line connecting its extrema. The z -velocity has been divided by the total velocity magnitude in the center of the cylinder, i.e. the points $(0, 0)$ in the graphs in Figure 4.15. The velocity field on the free surface is represent by arrows. At low angular velocity, the axial component of the velocity is less than 2% of the total; increasing Ω two areas with some axial flow start growing: the one toward the upper part of the free surface in which the flow is directed toward the center of the drum (warm colors in figures), and the one toward the lower part of the free surface in which the flow is directed toward the wall (cold colors in figures). The two parts are not symmetric: the upper one is bigger in size, but “weaker” than the lower one. The z -extent of these two areas are almost the same and increases with Ω .

Increasing the adherence at the wall will increase the strength of the axial flow, as shown in Figure 4.16. This is consistent with the observation made by Pohlman et al. (2006a) in cylinders with roughened end-walls and with DEM results by Chen et al. (2008)

4.8 Discussion

From results shown in the previous section, one can safely conclude that the JFP model describe dense granular flows in a consistent manner, thus it contains at least the basic elements of their physics. The most striking results come when comparing our results with experiments performed in similar operating conditions. In such a way we both demonstrate the predictive power of continuum simulations with the JFP model and also clarify to what extent the physics actually hidden behind experimental data can be caught in such a way. We compare our results with those of Félix et al. (2007), Alexander et al. (2002) and Pohlman et al. (2006a), since all of them used glass beads in their works.

Figure 4.17 shows the dimensionless thickness of the flowing layer against the angular velocity in a cylinder having $D/d_p = 1000$ and $AR = 0.1$. The cyan symbols from Félix et al. (2007) are the experimental flow depths at the wall of a cylinder having $D = 20cm$ and $W = 2cm$ half filled with particles having $d_p = 200\mu m$. Our numerical results are parametric in the degrees of slip; the magenta symbol represent the center of the range (reported as error bars) into which the flow layer at the center-plane falls at all slip parameter values. Solid lines are power laws with exponent equal to 0.37, which is the

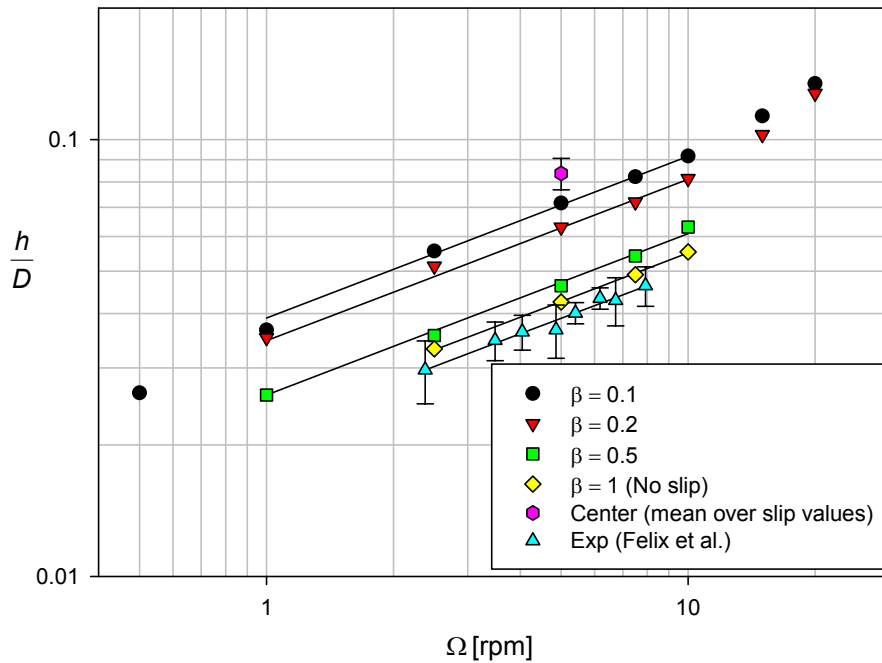


Figure 4.17: Comparison between our numerical results and experimental data by Félix et al. (2007). Numerical data regard the end wall of the cylinder; the error bar of the magenta hexagon represents the range of the flow depth at the center at all slip parameters. Solid lines are guides for the eye and have the slope declared by Félix et al. for the reported data set.

best fit declared by Félix et al. (2007) for their data.

As the wall slip is reduced, the numerical results get closer to the experimental values; the simulations with no-slip BC are in quantitative agreement with experiments. The wall slip effects saturates pretty fast: data at $\beta = 0.5$ are very close to those obtained with the adherence BC; it also has a very weak effect on what happens to the center of the cylinder.

This is, to the best of our knowledge, the first case in which fully 3D simulations with the JFP model quantitatively predict an actual experiment.

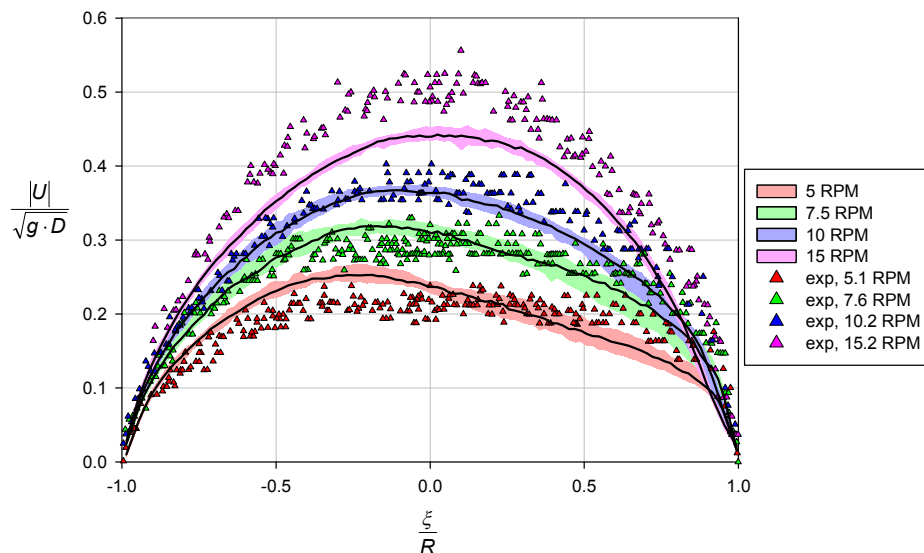


Figure 4.18: Comparison between our numerically predicted free-surface velocities at the center plane of the rotating cylinder and experimental data by Alexander et al. (2002). Shaded areas represent the 95% confidence intervals of our datasets.

An astonishing agreement is obtained near the end wall, where both the JFP model and the continuum hypothesis were considered prone to failures. The experimental results are strongly dependent on the presence of the wall and we also demonstrate the crucial role of the slip in determining the experimental outcome. In other words, experimental results in quasi-2D cylinders are actually those in which 3D effects are most important. This also questions the possibility of modeling of such flows in 2D.

Figure 4.18 shows the normalized velocity magnitude on the free surface versus the coordinate ξ (see Figure 4.15). The symbols are the experimental data obtained by Alexander et al. in a cylinder having $D/d_p = 155$ and $AR = 1.2$, the lines and the shaded colored areas are our numerical results (with $D/d_p = 1000$ and $AR = 1$) and estimates of their uncertainty. The

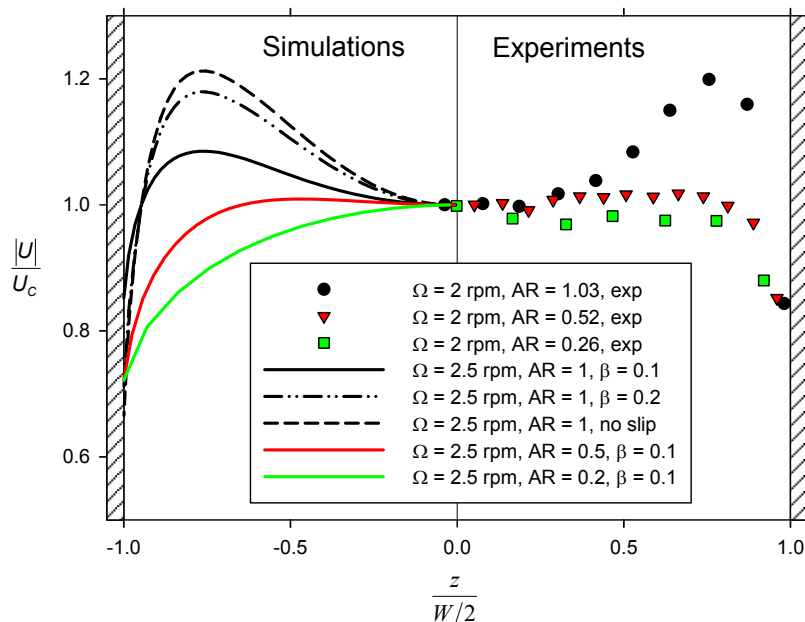


Figure 4.19: Comparison between numerical and experimental axial velocity profiles by (Pohlman et al., 2006a).

agreement is fair, even if both experiments and simulations show a noticeable scattering. Numerical velocity profiles show a maximum which moves towards the bottom of the free surface when Ω is increased; nevertheless Alexander et al. (2002) reports flatter profiles at low angular velocities. The agreement also demonstrates that the VoF method used here can fairly reproduce the actual behaviors on the free surface.

Another striking result come from the prediction of another wall-dominated experimental result. Data on the right-hand side of Figure 4.19 are the surface velocity profile along the axis of the cylinder measured by Pohlman et al. (2006a) for $D/d_p = 170$ and various aspect ratios. Our numerical results, shown in the left-hand side of Figure 4.19, concern cylinders having $D/d_p = 1000$. These numbers also represent the particles which would fit

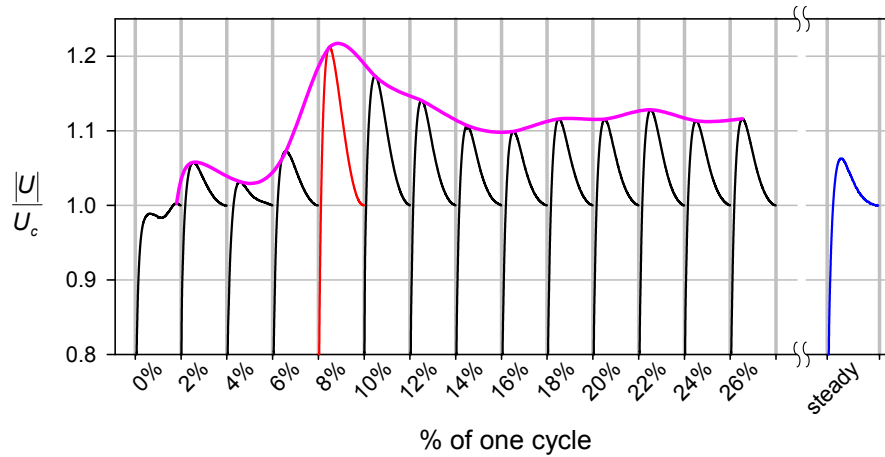


Figure 4.20: Time evolution of the axial velocity profile for the no-slip case. The red curve is the same as in Figure 4.19, the blue one is the steady (averaged) profile and the magenta curve is the time evolution of the velocity peak. The abscissa report the percentage of one complete turn starting from the onset of the flow.

in a cylinder with unitary aspect ratio: our simulations have almost 6 times more particles (in each direction) than the experiments.

There is a good agreement between simulations with no slip at the walls and experiments. As the aspect ratio is increased, the monotonic profile is lost and a peak can be observed near the wall. The peak becomes more and more pronounced as the adherence increases.

It must be noticed that their experiment design allow them to record data during the time needed by the cylinder to perform a quarter of a turn (from the onset of the flow). Our numerical velocity profiles have been taken in the same time window and are shown in Figure 4.20. Although the velocity peak observed tends to smear out approaching the steady state, reaching a value $\sim 5\%$ higher than the velocity at the center (see Figure 4.13), during

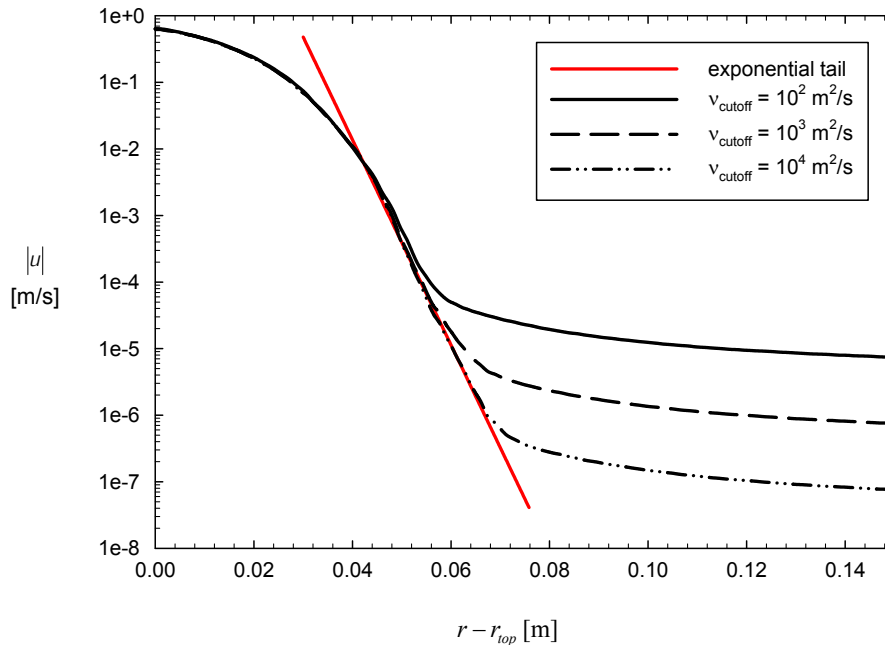


Figure 4.21: Velocity profiles, in the cylinder-fixed non-inertial reference frame, of a series of three simulations done with three different cutoff viscosities.

the time window available to experiments the profiles are quite close to those of Pohlman et al. (2006a).

The dependence of the peak height on adherence is consistent with the consideration made by Pohlman et al. that the peak is an end-wall effect and does not depend on particles size or geometry. Again, we could reproduce a distinctive feature of the interaction between the wall and the granular fluid thanks to the JFP model.

One of the critic point of the JFP model is that it might not predict the exponential tail found in velocity profiles in rotating cylinders: this criticality was indicated as a possible “failure” of the JFP model by model’s

author themselves (Jop et al., 2007; Pouliquen et al., 2006; Pouliquen and Forterre, 2009). Our simulations, however, do show such an exponential tail: Figure 4.21 reports the velocity profiles, in the cylinder-fixed non-inertial reference frame, of a series of three simulations done with three different cutoff viscosities (see Section 3.2). We can infer that the exponential tail does not depend on the chosen regularization, but is a true outcome of the physics simulated here: 3D simulations with the JFP model do account for the exponential tail of the velocity profile.

This is the very first time in which a quantitative agreement is obtained for dense grains in complex flow conditions. This demonstrates that the basic physics of the dense state is already captured by the simple JFP model and that the continuum mechanics can be used to get a physical insight in granular dense flow phenomena. We believe that CFD simulations with the JFP constitutive equation could in fact shed some light on a broad wealth of experimental results.

Conclusions

In this thesis we study the flow of dry, monodisperse granular materials in half-filled rotating cylinders in rolling regime by means of numerical simulations. The granular material is modeled as a continuum fluid with the JFP constitutive equation. We investigated the effects of the the ratio between the cylinder and particle diameter D/d_p , the ratio between the width and the diameter of the drum $AR = W/D$, the Froude number, which is a dimensionless angular velocity, and the degree of slip at the walls.

Most of the works devoted to the study of dry grains inside rotating drums focused their attention on the wall behavior of such systems (GDR MiDi, 2004) without accounting for its presence, even if the signature of the importance of wall effects is known to be crucial (Jop et al., 2005; Nakagawa et al., 1993; Parker et al., 1997). Indeed, the very first motivation of the JFP constitutive equation was to model the heap flow of granular material in presence of lateral walls. Nevertheless, few works are devoted to the description of the flow in wide cylinders and even less were able to probe granular materials inside the flowing zone, where the system is closed off to

optical apparati. Result from these experiments did show the essential 3D character of granular flow and the essential contribution of the walls on their flow behavior.

We tests our in-house implementation with the experimental results of different authors, finding a qualitatively and quantitatively agreement. We could match the velocity of glass beads along the free surface at the center plane of a wide drum, measured by Alexander et al. (2002), up to the angular velocity at which the system exits the rolling regime, where we underestimate the experiments. We also reproduced the characteristic non-linear profile reported by Pohlman et al. (2006a): the velocity is, somewhat counterintuitively, higher near the end walls of the cylinder than at its center. Even more dramatic is the fact that this agreement has been obtained during the initial transient, when the flow initiates. We also report the importance of the slip between the grains and the wall, which determine the height of the near-wall peak.

Our most striking results, in our opinion, was the excellent quantitative agreement with the experimental results of Félix et al. (2007). The authors measured the flow thickness at the wall of quasi-2D cylinders and reported a substantial independence of the flow thickness on the aspect ratio. We could not only quantitatively match their results on a cylinder with $AR = 0.1$, but we also observed that the wall flow depth is indeed nearly independent on AR and described the effect of the wall slip. This astonishing agreement is obtained on near-wall data, where not only the JFP model, but the overall continuum approach is supposed to be most prone to fail.

Furthermore, we could also observe a peculiar characteristic of granular

flows, i.e. the exponentially decreasing velocity tail in the fixed part of the flow, which have been reported in literature (Komatsu et al., 2001; Pouliquen et al., 2006; Jop et al., 2007; Pouliquen and Forterre, 2009).

On the minus side, we have not been able to capture neither the regime transition to the slumping regime, at low angular velocities, nor the transition to the cataracting regime, at high angular velocities, but only to get cues of such transitions. Regarding the former transition, we observed that, when the dynamic angle decreases below the repose angle, the system shows noticeable oscillations in all the probed quantities. These behaviors happen at angular velocities of the order of those theoretically predicted by Bouchaud et al. (1994) and Ding et al. (2002). On the other hand, instead of evolving into the cataracting regime, our simulations at high angular velocities show that the system attains very curved S -shaped interface with high inertial number values on the higher part of the free surface, where it is almost parallel to the lateral surface of the cylinder. We speculate that the transition might be triggered by a drop of the density of the system, which couldn't happen in our simulations since the density of the granular phase has been fixed. Future works might focus on the implementation of a density law for the granular material, i.e. the development of a *compressible* code for granular flow simulations.

Another point which needs further investigations is the refinement of the wall boundary conditions. Here a simple constant partial slip has been employed, while a wide variety of behaviors have been reported for granular materials near walls (i.e. stick-slip, Pöschel and Buchholtz, 1995; Buchholtz et al., 1995; Fried et al., 1998). Recently Artoni et al. (2009, 2012) focused

on how these behaviors can fit in a continuum framework and developed a boundary condition which is somewhat close to the partial slip BC here adopted. Implementing such new BC would be a challenging task for a future work.

In conclusion, our simulations demonstrate that the basic physics of the dense granular flow is captured by the simple JFP model, and that continuum mechanics can be used to get a physical insight in granular dense state phenomenology. CFD simulations may then be of help to rationalize the broad wealth of experimental results with these materials.

In a very recent numerical work, Chauchat and Médale (2014) concluded that *“another attractive direction for industrial or geophysical applications is to model free-surface flows, but the way to go is still long”*: in this thesis we demonstrated that we were closer to the target than Chauchat and Médale could imagine.

Bibliography

- A. Alexander, T. Shinbrot, and F. J. Muzzio, “Scaling surface velocities in rotating cylinders as a function of vessel radius, rotation rate, and particle size,” *Powder Technology*, vol. 126, no. 2, pp. 174–190, 2002.
- B. Andreotti, Y. Forterre, and O. Pouliquen, *Granular Media: Between Fluid and Solid*. Cambridge University Press, 2013.
- A. Aradian, E. Raphaël, and P.-G. de Gennes, “Thick surface flows of granular materials: Effect of the velocity profile on the avalanche amplitude,” *Physical Review E*, vol. 60, no. 2, pp. 2009–2019, 1999.
- R. Artoni, A. Santomaso, and P. Canu, “Effective boundary conditions for dense granular flows,” *Physical Review E*, vol. 79, no. 3, p. 031304, 2009.
- R. Artoni, A. C. Santomaso, M. Go’, and P. Canu, “Scaling laws for the slip velocity in dense granular flows,” *Physical Review Letters*, vol. 108, no. 23, p. 238002, 2012.
- E. Azéma and F. Radjai, “Internal structure of inertial granular flows,” *Physical Review Letters*, vol. 112, no. 7, p. 078001, 2014.
- E. Azéma, N. Estrada, and F. Radjai, “Nonlinear effects of particle shape angularity in sheared granular media,” *Physical Review E*, vol. 86, no. 4, p. 041301, 2012.

-
- R. A. Bagnold, “Experiments on a gravity-free dispersion of large solid spheres in a Newtonian fluid under shear,” *Proceedings of the Royal Society A: Mathematical, Physical and Engineering Sciences*, vol. 225, no. 1160, pp. 49–63, 1954.
- O. Baran, D. Ertas, T. Halsey, G. Grest, and J. Lechman, “Velocity correlations in dense gravity-driven granular chute flow,” *Physical Review E*, vol. 74, no. 5, p. 051302, 2006.
- E. Berberović, N. van Hinsberg, S. Jakirlić, I. Roisman, and C. Tropea, “Drop impact onto a liquid layer of finite thickness: Dynamics of the cavity evolution,” *Physical Review E*, vol. 79, no. 3, p. 036306, 2009.
- D. Berzi, “Extended kinetic theory applied to dense, granular, simple shear flows,” *Acta Mech*, vol. 225, no. 8, pp. 2191–2198, 2014.
- D. Berzi and J. T. Jenkins, “Surface flows of inelastic spheres,” *Physics of Fluids*, vol. 23, no. 1, p. 013303, 2011.
- P. Boltenhagen, “Boundary effects on the maximal angle of stability of a granular packing,” *European Physical Journal B: Condensed Matter and Complex Systems*, vol. 12, no. 1, pp. 75–78, 1999.
- D. Bonamy, F. Daviaud, and L. Laurent, “Experimental study of granular surface flows via a fast camera: A continuous description,” *Physics of Fluids*, vol. 14, no. 5, p. 1666, 2002.
- D. Bonamy, F. Daviaud, L. Laurent, M. Bonetti, and J. Bouchaud, “Multi-scale clustering in granular surface flows,” *Physical Review Letters*, vol. 89, no. 3, p. 034301, 2002.
- J.-P. Bouchaud, M. E. Cates, J. Ravi Prakash, and S. F. Edwards, “A model for the dynamics of sandpile surfaces,” *Journal de Physique I*, vol. 4, no. 10, pp. 1383–1410, 1994.
- T. Boutreux, E. Raphaël, and P.-G. de Gennes, “Surface flows of granular materials: A modified picture for thick avalanches,” *Physical Review E*, vol. 58, no. 4, pp. 4692–4700, 1998.

-
- M. Bouzid, M. Trulsson, P. Claudin, E. Clément, and B. Andreotti, “Nonlocal rheology of granular flows across yield conditions,” *Physical Review Letters*, vol. 111, no. 23, p. 238301, 2013.
- V. Buchholtz, T. Pöschel, and H.-J. Tillemans, “Simulation of rotating drum experiments using non-circular particles,” *Physica A: Statistical Mechanics and its Applications*, vol. 216, no. 3, pp. 199–212, 1995.
- C. S. Campbell, “Rapid granular flows,” *Annual Review of Fluid Mechanics*, vol. 22, no. 1, pp. 57–90, 1990.
- G. Chambon, R. Bouvarel, D. Laigle, and M. Naaim, “Numerical simulations of granular free-surface flows using smoothed particle hydrodynamics,” *Journal of Non-Newtonian Fluid Mechanics*, vol. 166, no. 12-13, pp. 698–712, 2011.
- J. Chauchat and M. Médale, “A three-dimensional numerical model for dense granular flows based on the $\mu(I)$ rheology,” *Journal of Computational Physics*, vol. 256, pp. 696–712, 2014.
- P. Chen, J. Ottino, and R. Lueptow, “Subsurface granular flow in rotating tumblers: A detailed computational study,” *Physical Review E*, vol. 78, no. 2, p. 021303, 2008.
- H.-T. Chou and C.-F. Lee, “Cross-sectional and axial flow characteristics of dry granular material in rotating drums,” *Granular Matter*, vol. 11, no. 1, pp. 13–32, 2008.
- P.-P. Cortet, D. Bonamy, F. Daviaud, O. Dauchot, B. Dubrulle, and M. Renouf, “Relevance of visco-plastic theory in a multi-directional inhomogeneous granular flow,” *Europhysics Letters*, vol. 88, no. 1, p. 14001, 2009.
- S. Courrech du Pont, P. Gondret, B. Perrin, and M. Rabaud, “Wall effects on granular heap stability,” *Europhysics Letters*, vol. 61, no. 4, pp. 492–498, 2003.
- P. A. Cundall and O. D. L. Strack, “A discrete numerical model for granular assemblies,” *Géotechnique*, vol. 29, no. 1, pp. 47–65, 1979.

-
- F. da Cruz, S. Emam, M. Prochnow, J.-N. Roux, and F. Chevoir, “Rheo-
physics of dense granular materials: Discrete simulation of plane shear
flows,” *Physical Review E*, vol. 72, no. 2, p. 021309, 2005.
- P.-G. de Gennes, “Granular matter: a tentative view,” *Reviews of Modern
Physics*, vol. 71, no. 2, pp. S374–S382, 1999.
- Y. Demagh, H. Ben Moussa, M. Lachi, S. Noui, and L. Bordja, “Surface
particle motions in rotating cylinders: Validation and similarity for an
industrial scale kiln,” *Powder Technology*, vol. 224, pp. 260–272, 2012.
- M. Depken, W. van Saarloos, and M. van Hecke, “Continuum approach
to wide shear zones in quasistatic granular matter,” *Physical Review E*,
vol. 73, no. 3, p. 031302, 2006.
- S. S. Deshpande, L. Anumolu, and M. F. Trujillo, “Evaluating the perfor-
mance of the two-phase flow solver interfoam,” *Computational Science &
Discovery*, vol. 5, no. 1, p. 014016, 2012.
- Y. Ding, J. Seville, R. Forster, and D. Parker, “Solids motion in rolling mode
rotating drums operated at low to medium rotational speeds,” *Chemical
Engineering Science*, vol. 56, no. 5, pp. 1769–1780, 2001.
- Y. Ding, R. Forster, J. Seville, and D. Parker, “Granular motion in rotat-
ing drums: bed turnover time and slumping–rolling transition,” *Powder
Technology*, vol. 124, no. 1-2, pp. 18–27, 2002.
- S. Douady, B. Andreotti, and A. Daerr, “On granular surface flow equations,”
European Physical Journal B: Condensed Matter and Complex Systems,
vol. 11, no. 1, pp. 131–142, 1999.
- C. Dury, G. Ristow, J. Moss, and M. Nakagawa, “Boundary effects on the
angle of repose in rotating cylinders,” *Physical Review E*, vol. 57, no. 4,
pp. 4491–4497, 1998.
- A. N. Edwards and J. M. N. T. Gray, “Erosion–deposition waves in shallow
granular free–surface flows,” *Journal of Fluid Mechanics*, vol. 762, pp. 35–
67, 2015.

-
- T. Elperin and A. Vikhansky, “Granular flow in a rotating cylindrical drum,” *Europhysics Letters*, vol. 42, no. 6, pp. 619–624, 1998.
- A. Faqih, B. Chaudhuri, F. J. Muzzio, M. S. Tomassone, A. Alexander, and S. Hammond, “Flow-induced dilation of cohesive granular materials,” *AIChE Journal*, vol. 52, no. 12, pp. 4124–4132, 2006.
- G. Félix, V. Falk, and U. D’Ortona, “Granular flows in a rotating drum: the scaling law between velocity and thickness of the flow,” *The European Physical Journal E*, vol. 22, no. 1, pp. 25–31, 2007.
- J. H. Ferziger and M. Perić, *Computational Methods for Fluid Dynamics*, 3rd ed. Springer Berlin Heidelberg, 2001.
- Y. Forterre, “Kapiza waves as a test for three-dimensional granular flow rheology,” *Journal of Fluid Mechanics*, vol. 563, p. 123, 2006.
- Y. Forterre and O. Pouliquen, “Long-surface-wave instability in dense granular flows,” *Journal of Fluid Mechanics*, vol. 486, pp. 21–50, 2003.
- , “Flows of dense granular media,” *Annual Review of Fluid Mechanics*, vol. 40, no. 1, pp. 1–24, 2008.
- F. Franklin and L. Johanson, “Flow of granular material through a circular orifice,” *Chemical Engineering Science*, vol. 4, no. 3, pp. 119–129, 1955.
- E. Fried, A. Q. Shen, and S. T. Thoroddsen, “Wave patterns in a thin layer of sand within a rotating horizontal cylinder,” *Physics of Fluids*, vol. 10, no. 1, p. 10, 1998.
- GDR MiDi, “On dense granular flows,” *The European Physical Journal E*, vol. 14, no. 4, pp. 341–365, 2004.
- C. Goldenberg, A. Atman, P. Claudin, G. Combe, and I. Goldhirsch, “Scale separation in granular packings: Stress plateaus and fluctuations,” *Physical Review Letters*, vol. 96, no. 16, p. 168001, 2006.

-
- I. Goldhirsch, “Rapid granular flows,” *Annual Review of Fluid Mechanics*, vol. 35, no. 1, pp. 267–293, 2003.
- J. Gollub, “Discrete and continuum descriptions of matter,” *Physics Today*, vol. 56, no. 1, pp. 10–11, 2003.
- Y. Grasselli and H. Herrmann, “On the angles of dry granular heaps,” *Physica A: Statistical Mechanics and its Applications*, vol. 246, no. 3-4, pp. 301–312, 1997.
- J. M. N. T. Gray and A. N. Edwards, “A depth-averaged $\mu(I)$ -rheology for shallow granular free-surface flows,” *Journal of Fluid Mechanics*, vol. 755, pp. 503–534, 2014.
- P. K. Haff, “Grain flow as a fluid-mechanical phenomenon,” *Journal of Fluid Mechanics*, vol. 134, p. 401, 1983.
- D. L. Henann and K. Kamrin, “Continuum modeling of secondary rheology in dense granular materials,” *Physical Review Letters*, vol. 113, no. 17, p. 178001, 2014.
- H. Henein, J. K. Brimacombe, and A. P. Watkinson, “Experimental study of transverse bed motion in rotary kilns,” *Metallurgical Transactions B*, vol. 14, no. 2, pp. 191–205, 1983.
- C. Hirt and B. Nichols, “Volume of fluid (vof) method for the dynamics of free boundaries,” *Journal of Computational Physics*, vol. 39, no. 1, pp. 201–225, 1981.
- A.-N. Huang, W.-C. Kao, and H.-P. Kuo, “Numerical studies of particle segregation in a rotating drum based on Eulerian continuum approach,” *Advanced Powder Technology*, vol. 24, no. 1, pp. 364–372, 2013.
- R. Issa, A. Gosman, and A. Watkins, “The computation of compressible and incompressible recirculating flows by a non-iterative implicit scheme,” *Journal of Computational Physics*, vol. 62, no. 1, pp. 66–82, 1986.

-
- H. Jaeger, C.-h. Liu, and S. Nagel, “Relaxation at the angle of repose,” *Physical Review Letters*, vol. 62, no. 1, pp. 40–43, 1989.
- H. Jaeger, S. Nagel, and R. Behringer, “Granular solids, liquids, and gases,” *Reviews of Modern Physics*, vol. 68, no. 4, pp. 1259–1273, 1996.
- N. Jain, J. M. Ottino, and R. M. Lueptow, “An experimental study of the flowing granular layer in a rotating tumbler,” *Physics of Fluids*, vol. 14, no. 2, p. 572, 2002.
- , “Effect of interstitial fluid on a granular flowing layer,” *Journal of Fluid Mechanics*, vol. 508, pp. 23–44, 2004.
- M. Jean, “The non-smooth contact dynamics method,” *Computer Methods in Applied Mechanics and Engineering*, vol. 177, no. 3-4, pp. 235–257, 1999.
- J. T. Jenkins, “Dense inclined flows of inelastic spheres,” *Granular Matter*, vol. 10, no. 1, pp. 47–52, 2007.
- J. T. Jenkins and D. Berzi, “Dense inclined flows of inelastic spheres: tests of an extension of kinetic theory,” *Granular Matter*, vol. 12, no. 2, pp. 151–158, 2010.
- P. Jop, “Hydrodynamic modeling of granular flows in a modified couette cell,” *Physical Review E*, vol. 77, no. 3, p. 032301, 2008.
- P. Jop, Y. Forterre, and O. Pouliquen, “Crucial role of sidewalls in granular surface flows: consequences for the rheology,” *Journal of Fluid Mechanics*, vol. 541, p. 167, 2005.
- , “A constitutive law for dense granular flows,” *Nature*, vol. 441, no. 7094, pp. 727–730, 2006.
- , “Initiation of granular surface flows in a narrow channel,” *Physics of Fluids*, vol. 19, no. 8, p. 088102, 2007.
- L. Kadanoff, “Built upon sand: Theoretical ideas inspired by granular flows,” *Reviews of Modern Physics*, vol. 71, no. 1, pp. 435–444, 1999.

-
- K. Kamrin and G. Koval, “Nonlocal constitutive relation for steady granular flow,” *Physical Review Letters*, vol. 108, no. 17, p. 178301, 2012.
- D. V. Khakhar, J. J. McCarthy, T. Shinbrot, and J. M. Ottino, “Transverse flow and mixing of granular materials in a rotating cylinder,” *Physics of Fluids*, vol. 9, no. 1, p. 31, 1997.
- M. Khalilitehrani, P. J. Abrahamsson, and A. Rasmuson, “The rheology of dense granular flows in a disc impeller high shear granulator,” *Powder Technology*, vol. 249, pp. 309–315, 2013.
- T. Komatsu, S. Inagaki, N. Nakagawa, and S. Nasuno, “Creep motion in a granular pile exhibiting steady surface flow,” *Physical Review Letters*, vol. 86, no. 9, pp. 1757–1760, 2001.
- H. Kramers and P. Croockewit, “The passage of granular solids through inclined rotary kilns,” *Chemical Engineering Science*, vol. 1, no. 6, pp. 259–265, 1952.
- L. Lacaze and R. Kerswell, “Axisymmetric granular collapse: A transient 3D flow test of viscoplasticity,” *Physical Review Letters*, vol. 102, no. 10, p. 108305, 2009.
- P.-Y. Lagrée, L. Staron, and S. Popinet, “The granular column collapse as a continuum: validity of a two-dimensional navier–stokes model with a $\mu(I)$ -rheology,” *Journal of Fluid Mechanics*, vol. 686, pp. 378–408, 2011.
- E. Lajeunesse, A. Mangeney-Castelnau, and J. P. Vilotte, “Spreading of a granular mass on a horizontal plane,” *Physics of Fluids*, vol. 16, no. 7, p. 2371, 2004.
- J.-P. Longmore, P. Marais, and M. M. Kuttel, “Towards realistic and interactive sand simulation: A GPU-based framework,” *Powder Technology*, vol. 235, pp. 983–1000, 2013.
- G. Lube, H. E. Huppert, R. S. J. Sparks, and M. A. Hallworth, “Axisymmetric collapses of granular columns,” *Journal of Fluid Mechanics*, vol. 508, pp. 175–199, 2004.

-
- H. Makse, “Continuous avalanche segregation of granular mixtures in thin rotating drums,” *Physical Review Letters*, vol. 83, no. 16, pp. 3186–3189, 1999.
- J. E. Maneval, K. M. Hill, B. E. Smith, A. Caprihan, and E. Fukushima, “Effects of end wall friction in rotating cylinder granular flow experiments,” *Granular Matter*, vol. 7, no. 4, pp. 199–202, 2005.
- S. W. Meier, R. M. Lueptow, and J. M. Ottino, “A dynamical systems approach to mixing and segregation of granular materials in tumblers,” *Advances in Physics*, vol. 56, no. 5, pp. 757–827, 2007.
- J. Mellmann, “The transverse motion of solids in rotating cylinders—forms of motion and transition behavior,” *Powder Technology*, vol. 118, no. 3, pp. 251–270, 2001.
- G. Metcalfe and M. Shattuck, “Pattern formation during mixing and segregation of flowing granular materials,” *Physica A: Statistical Mechanics and its Applications*, vol. 233, no. 3-4, pp. 709–717, 1996.
- L. Minatti and E. Paris, “A sph model for the simulation of free surface granular flows in a dense regime,” *Applied Mathematical Modelling*, vol. 39, no. 1, pp. 363–382, 2015.
- M. Nakagawa, S. Altobelli, A. Caprihan, E. Fukushima, and E.-K. Jeong, “Non-invasive measurements of granular flows by magnetic resonance imaging,” *Experiments in Fluids*, vol. 16, no. 1, pp. 54–60, 1993.
- M. Nakagawa, “Axial segregation of granular flows in a horizontal rotating cylinder,” *Chemical Engineering Science*, vol. 49, no. 15, pp. 2540–2544, 1994.
- M. Nakagawa, S. A. Altobelli, A. Caprihan, and E. Fukushima, “Nmri study: axial migration of radially segregated core of granular mixtures in a horizontal rotating cylinder,” *Chemical Engineering Science*, vol. 52, no. 23, pp. 4423–4428, 1997.

-
- A. Orpe and D. Khakhar, “Scaling relations for granular flow in quasi-two-dimensional rotating cylinders,” *Physical Review E*, vol. 64, no. 3, p. 031302, 2001.
- A. V. Orpe and D. V. Khakhar, “Rheology of surface granular flows,” *Journal of Fluid Mechanics*, vol. 571, p. 1, 2007.
- J. M. Ottino and D. V. Khakhar, “Mixing and segregation of granular materials,” *Annual Review of Fluid Mechanics*, vol. 32, no. 1, pp. 55–91, 2000.
- J. M. Ottino, “Granular matter as a window into collective systems far from equilibrium, complexity, and scientific prematurity,” *Chemical Engineering Science*, vol. 61, no. 13, pp. 4165–4171, 2006.
- D. J. Parker, X. Fan, R. N. G. Forster, P. Fowles, Y. Ding, and J. P. K. Seville, “Positron imaging studies of rotating drums,” *The Canadian Journal of Chemical Engineering*, vol. 83, no. 1, pp. 83–87, 2005.
- D. Parker, A. Dijkstra, T. Martin, and J. Seville, “Positron emission particle tracking studies of spherical particle motion in rotating drums,” *Chemical Engineering Science*, vol. 52, no. 13, pp. 2011–2022, 1997.
- S. V. Patankar, *Numerical heat transfer and fluid flow*, ser. Hemisphere Series on Computational Methods in Mechanics and Thermal Science, M. A. Phillips and E. M. Millman, Eds. CRC Press, 1980.
- P.-E. Peyneau and J.-N. Roux, “Frictionless bead packs have macroscopic friction, but no dilatancy,” *Physical Review E*, vol. 78, no. 1, p. 011307, 2008.
- F. Pignatelli, C. Asselin, L. Krieger, I. C. Christov, J. M. Ottino, and R. M. Lueptow, “Parameters and scalings for dry and immersed granular flowing layers in rotating tumblers,” *Physical Review E*, vol. 86, no. 1, p. 011304, 2012.
- N. Pohlman, S. W. Meier, R. Lueptow, and J. Ottino, “Surface velocity in three-dimensional granular tumblers,” *Journal of Fluid Mechanics*, vol. 560, pp. 355–368, 2006.

-
- N. Pohlman, J. Ottino, and R. Lueptow, “End–wall effects in granular tumblers: From quasi–two–dimensional flow to three–dimensional flow,” *Physical Review E*, vol. 74, no. 3, p. 031305, 2006.
- N. Pohlman, B. Severson, J. Ottino, and R. Lueptow, “Surface roughness effects in granular matter: Influence on angle of repose and the absence of segregation,” *Physical Review E*, vol. 73, no. 3, p. 031304, 2006.
- T. Pöschel and V. Buchholtz, “Complex flow of granular material in a rotating cylinder,” *Chaos, Solitons & Fractals*, vol. 5, no. 10, pp. 1901–1912, 1995.
- O. Pouliquen, C. Cassar, P. Jop, Y. Forterre, and M. Nicolas, “Flow of dense granular material: towards simple constitutive laws,” *Journal of Statistical Mechanics: Theory and Experiment*, vol. 2006, no. 07, p. P07020, 2006.
- O. Pouliquen, “Scaling laws in granular flows down rough inclined planes,” *Physics of Fluids*, vol. 11, no. 3, pp. 542–548, 1999.
- O. Pouliquen and Y. Forterre, “Friction law for dense granular flows: application to the motion of a mass down a rough inclined plane,” *Journal of Fluid Mechanics*, vol. 453, pp. 133–151, 2002.
- , “A non–local rheology for dense granular flows,” *Philosophical Transactions of the Royal Society A: Mathematical, Physical and Engineering Sciences*, vol. 367, no. 1909, pp. 5091–5107, 2009.
- J. Rajchenbach, “Flow in powders: From discrete avalanches to continuous regime,” *Physical Review Letters*, vol. 65, no. 18, pp. 2221–2224, 1990.
- M. Renouf, D. Bonamy, F. Dubois, and P. Alart, “Numerical simulation of two–dimensional steady granular flows in rotating drum: On surface flow rheology,” *Physics of Fluids*, vol. 17, no. 10, p. 103303, 2005.
- O. Reynolds, “Lvii. on the dilatancy of media composed of rigid particles in contact. with experimental illustrations,” *Philosophical Magazine Series 5*, vol. 20, no. 127, pp. 469–481, 1885.

-
- G. H. Ristow, “Dynamics of granular materials in a rotating drum,” *Europhysics Letters*, vol. 34, no. 4, pp. 263–268, 1996.
- J.-N. Roux and G. Combe, “Quasistatic rheology and the origins of strain,” *Comptes Rendus Physique*, vol. 3, no. 2, pp. 131–140, 2002.
- C. H. Rycroft, K. Kamrin, and M. Z. Bazant, “Assessing continuum postulates in simulations of granular flow,” *Journal of the Mechanics and Physics of Solids*, vol. 57, no. 5, pp. 828–839, 2009.
- L. Sanfratello, A. Caprihan, and E. Fukushima, “Velocity depth profile of granular matter in a horizontal rotating drum,” *Granular Matter*, vol. 9, no. 1-2, pp. 1–6, 2006.
- S. B. Savage and K. Hutter, “The motion of a finite mass of granular material down a rough incline,” *Journal of Fluid Mechanics*, vol. 199, p. 177, 1989.
- S. B. Savage, “Gravity flow of cohesionless granular materials in chutes and channels,” *Journal of Fluid Mechanics*, vol. 92, no. 1, pp. 53–96, 1979.
- , “The mechanics of rapid granular flows,” *Advances in Applied Mechanics*, vol. 24, pp. 289–366, 1984.
- “What we don’t know?” *Science*, vol. 309, no. 5731, pp. 78–102, 2005.
- D. Scott, J. Davidson, S.-Y. Lim, and R. Spurling, “Flow of granular material through an inclined, rotating cylinder fitted with a dam,” *Powder Technology*, vol. 182, no. 3, pp. 466–473, 2008.
- G. Seiden and P. J. Thomas, “Complexity, segregation, and pattern formation in rotating-drum flows,” *Reviews of Modern Physics*, vol. 83, no. 4, pp. 1323–1365, 2011.
- L. Silbert, D. Ertas, G. Grest, T. Halsey, D. Levine, and S. Plimpton, “Granular flow down an inclined plane: Bagnold scaling and rheology,” *Physical Review E*, vol. 64, no. 5, p. 051302, 2001.

-
- L. Staron, P.-Y. Lagrée, and S. Popinet, “The granular silo as a continuum plastic flow: The hour-glass vs the clepsydra,” *Physics of Fluids*, vol. 24, no. 10, p. 103301, 2012.
- L. Staron, P. Y. Lagrée, and S. Popinet, “Continuum simulation of the discharge of the granular silo,” *The European Physical Journal E*, vol. 37, no. 1, p. 5, 2014.
- J. Sun and S. Sundaresan, “A constitutive model with microstructure evolution for flow of rate-independent granular materials,” *Journal of Fluid Mechanics*, vol. 682, pp. 590–616, 2011.
- N. Taberlet, P. Richard, A. Valance, W. Losert, J. Pasini, J. Jenkins, and R. Delannay, “Superstable granular heap in a thin channel,” *Physical Review Letters*, vol. 91, no. 26, p. 264301, 2003.
- N. Taberlet, P. Richard, and E. John Hinch, “S shape of a granular pile in a rotating drum,” *Physical Review E*, vol. 73, no. 5, p. 050301, 2006.
- J. R. Third, D. M. Scott, S. A. Scott, and C. R. Müller, “Tangential velocity profiles of granular material within horizontal rotating cylinders modelled using the DEM,” *Granular Matter*, vol. 12, no. 6, pp. 587–595, 2010.
- L. Våhl and W. Kingma, “Transport of solids through horizontal rotary cylinders,” *Chemical Engineering Science*, vol. 1, no. 6, pp. 253–258, 1952.
- S. Vun, J. Naser, and P. Witt, “Extension of the kinetic theory of granular flow to include dense quasi-static stresses,” *Powder Technology*, vol. 204, no. 1, pp. 11–20, 2010.
- H. G. Weller, G. Tabor, H. Jasak, and C. Fureby, “A tensorial approach to computational continuum mechanics using object-oriented techniques,” *Computers in Physics*, vol. 12, no. 6, p. 620, 1998.
- K. Yamane, M. Nakagawa, S. A. Altobelli, T. Tanaka, and Y. Tsuji, “Steady particulate flows in a horizontal rotating cylinder,” *Physics of Fluids*, vol. 10, no. 6, p. 1419, 1998.

- R. Yang, R. Zou, and A. Yu, “Microdynamic analysis of particle flow in a horizontal rotating drum,” *Powder Technology*, vol. 130, no. 1-3, pp. 138–146, 2003.
- Q. Zheng and A. Yu, “Why have continuum theories previously failed to describe sandpile formation?” *Physical Review Letters*, vol. 113, no. 6, p. 068001, 2014.
- H. Zhu, Z. Zhou, R. Yang, and A. Yu, “Discrete particle simulation of particulate systems: Theoretical developments,” *Chemical Engineering Science*, vol. 62, no. 13, pp. 3378–3396, 2007.
- , “Discrete particle simulation of particulate systems: A review of major applications and findings,” *Chemical Engineering Science*, vol. 63, no. 23, pp. 5728–5770, 2008.
- O. Zik, D. Levine, S. Lipson, S. Shtrikman, and J. Stavans, “Rotationally induced segregation of granular materials,” *Physical Review Letters*, vol. 73, no. 5, pp. 644–647, 1994.